algorithms

MDPI

Article

Deep Neural Networks Training by Stochastic Quasi-Newton Trust-Region Methods

Mahsa Yousefi and Ángeles Martínez *

Department of Mathematics and Geoscienzes, University of Trieste, 34127 Trieste, Italy; mahsa.yousefi@phd.units.it
* Correspondence: amartinez@units.it

Abstract: While first-order methods are popular for solving optimization problems arising in deep learning, they come with some acute deficiencies. To overcome these shortcomings, there has been recent interest in introducing second-order information through quasi-Newton methods that are able to construct Hessian approximations using only gradient information. In this work, we study the performance of stochastic quasi-Newton algorithms for training deep neural networks. We consider two well-known quasi-Newton updates, the limited-memory Broyden–Fletcher–Goldfarb–Shanno (BFGS) and the symmetric rank one (SR1). This study fills a gap concerning the real performance of both updates in the minibatch setting and analyzes whether more efficient training can be obtained when using the more robust BFGS update or the cheaper SR1 formula, which—allowing for indefinite Hessian approximations—can potentially help to better navigate the pathological saddle points present in the non-convex loss functions found in deep learning. We present and discuss the results of an extensive experimental study that includes many aspects affecting performance, like batch normalization, the network architecture, the limited memory parameter or the batch size. Our results show that stochastic quasi-Newton algorithms are efficient and, in some instances, able to outperform the well-known first-order Adam optimizer, run with the optimal combination of its numerous hyperparameters, and the stochastic second-order trust-region STORM algorithm.

Keywords: stochastic optimization; quasi-Newton methods; trust-region methods; BFGS; SR1; deep neural networks training

MSC: 90C30; 90C06; 90C53; 90C90; 65K05

check for updates

Citation: Yousefi, M.; Martínez, Á. Deep Neural Networks Training by Stochastic Quasi-Newton Trust-Region Methods. *Algorithms* **2023**, *16*, 490. https://doi.org/10.3390/a16100490

Academic Editors: Sona Taheri, Kaisa Joki, Yury Nikulin and Napsu Karmitsa

Received: 25 September 2023
Revised: 14 October 2023
Accepted: 16 October 2023
Published: 20 October 2023

Copyright: © 2023 by the authors. Licensee MDPI, Basel, Switzerland. This article is an open access article distributed under the terms and conditions of the Creative Commons Attribution (CC BY) license (https://creativecommons.org/licenses/by/4.0/).

1. Introduction

Deep learning (DL), as a leading technique of machine learning (ML), has attracted much attention and has become one of the most popular directions of research. DL approaches have been applied to solve many large-scale problems in different fields, e.g., automatic machine translation, image recognition, natural language processing, fraud detection, etc., by training deep neural networks (DNNs) over large available datasets. DL problems are often posed as unconstrained optimization problems. In supervised learning, the goal is to minimize the empirical risk:

$$\min_{w\in\mathbb{R}^n} F(w) \triangleq \frac{1}{N}\sum_{i=1}^{N} L(y_i, h(x_i;w)) \triangleq \frac{1}{N}\sum_{i=1}^{N} L_i(w), \tag{1}$$

by finding an optimal parametric mapping function $h(\cdot;w) : \mathbb{R}^d \longrightarrow \mathbb{R}^C$, where $w \in \mathbb{R}^n$ is the vector of the trainable parameters of a DNN and (x_i, y_i) denotes the ith sample pair in the available training dataset $\{(x_i, y_i)\}_{i=1}^N$ with converted input $x_i \in \mathbb{R}^d$ and a one-hot true target $y_i \in \mathbb{R}^C$. Moreover, $L_i(.,.) \in \mathbb{R}$ is a loss function defining the prediction error between y_i and the DNN's output $h(x_i;.)$. Problem (1) is highly nonlinear and often non-convex and, thus, applying traditional optimization algorithms is ineffective.

Optimization methods for problem (1) can be divided into *first-order* and *second-order* methods, where the gradient and Hessian (or a Hessian approximation) are used, respectively. These methods, in turn, fall into two broad categories, stochastic and deterministic, in which either one sample (or a small subset of samples called minibatch) or a single batch composed of all samples are, respectively, employed in the evaluation of the objective function or its gradient.

In DL applications, both N and n can be very large; thus, computing the full gradient is expensive, and computations involving the true Hessian or its approximation may not be practical. Recently, much effort has been devoted to the development of DL optimization algorithms. Stochastic optimization methods have become the usual approach to overcoming the aforementioned issues.

1.1. Review of the Literature

Stochastic first-order methods have been widely used in many DL applications, due to their low per-iteration cost, optimal complexity, easy implementation, and proven efficiency in practice. The preferred method is the stochastic gradient descent (SGD) method [1,2], and its variance-reduced [3–5] and adaptive [6,7] variants. However, due to the use of first-order information only, these methods come with several issues, such as relatively slow convergence, high sensitivity to the choice of hyperparameters (e.g., step length and batch size), stagnation at high training loss, difficulty in escaping saddle points [8], the limited benefits of parallelism, due to the usual implementation with small minibatches, and suffering from ill-conditioning [9].

On the other hand, second-order methods can often find good minima in fewer steps, due to their use of curvature information. The main second-order method incorporating the inverse Hessian matrix is Newton's method [10], but it presents serious computational and memory usage challenges involved in the computation of the Hessian, in particular for large-scale DL problems; see [11] for details.

Quasi-Newton [10] and Hessian-free Newton methods [12] are two techniques aimed at incorporating second-order information without computing and storing the true Hessian matrix. Hessian-free methods attempt to find an approximate Newton direction, using conjugate gradient methods [13–15]. The major challenge of these methods is the linear system with an indefinite subsampled Hessian matrix and (subsampled) gradient vector to be solved at each Newton step. This problem can be solved in the trust region framework by the CG–Steihaug algorithm [16]. Nevertheless, whether true Hessian matrix–vector products or subsampled variants of them (see, e.g., [15]) are used, the iteration complexity of a (modified) CG algorithm is significantly greater than that of a limited-memory quasi-Newton method, i.e., stochastic L-BFGS; see the complexity table in [15]. Quasi-Newton methods and their limited memory variants [10] attempt to combine the speed of Newton's method and the scalability of first-order methods. They construct Hessian approximations, using only gradient information, and they exhibit superlinear convergence. All these methods can be implemented to benefit from parallelization in the evaluations of the objective function and its derivatives, which is possible, due to their finite sum structure [11,17,18].

Quasi-Newton and stochastic quasi-Newton methods to solve large optimization problems arising in machine learning have been recently extensively considered within the context of convex and non-convex optimization. Stochastic quasi-Newton methods use a subsampled Hessian approximation or/and a subsampled gradient. In [19], a stochastic Broyden–Fletcher–Goldfarb–Shanno (BFGS) and its limited memory variant (L-BFGS) were proposed for online convex optimization in [19]. Another stochastic L-BFGS method for solving strongly convex problems was presented in [20] that uses sampled Hessian-vector products rather than gradient differences, which was proved in [21] to be linearly convergent by incorporating the SVRG variance reduction technique [4] to alleviate the effect of noisy gradients. A closely related variance-reduced block L-BFGS method was proposed in [22]. A regularized stochastic BFGS method was proposed in [23], and an online L-BFGS method was proposed in [24] for strongly convex problems and extended

in [25] to incorporate SVRG variance reduction. For the solution of non-convex optimization problems arising in deep learning, a damped L-BFGS method incorporating SVRG variance reduction was developed and its convergence properties were studied in [26]. Some of these stochastic quasi-Newton algorithms employ fixed-size batches and compute stochastic gradient differences in a stable way, originally proposed in [19], using the same batch at the beginning and at the end of the iteration. As this can potentially double the iteration complexity, an overlap batching strategy was proposed, to reduce the computational cost in [27], and it was also tested, in [28]. This strategy was further applied in [29,30]. Other stochastic quasi-Newton methods have been considered that employ a progressive batching approach in which the sample size is increased as the iteration progresses; see, e.g., [31,32] and references therein. Recently, in [33], a Kronecker-factored block diagonal BFGS and L-BFGS method was proposed, which takes advantage of the structure of feed-forward DNN training problems.

1.2. Contribution and Outline

The BFGS update is the most widely used type of quasi-Newton method for general optimization and the most widely considered quasi-Newton method for general machine learning and deep learning. Almost all the previously cited articles considered BFGS, with only a few exceptions using the symmetric rank one (SR1) update instead [29]. However, a clear disadvantage of BFGS occurs if one tries to enforce the positive-definiteness of the approximated Hessian matrices in a non-convex setting. In this case, BFGS has the difficult task of approximating an indefinite matrix (the true Hessian) with a positive-definite matrix which can result in the generation of nearly singular Hessian approximations.

In this paper, we analyze the behavior of both updates on real modern deep neural network architectures and try to determine whether more efficient training can be obtained when using the BFGS update or the cheaper SR1 formula that allows for indefinite Hessian approximations and, thus, can potentially help to better navigate the pathological saddle points present in the non-convex loss functions found in deep learning. We would like to determine whether better training results could be achieved by using SR1 updates, as these allow for indefinite Hessian approximations. We study the performance of both quasi-Newton methods in the trust region framework for solving (1) in realistic large-size DNNs. We introduce stochastic variants of the two quasi-Newton updates, based on an overlapping sampling strategy which is well-suited to trust-region methods. We have implemented and applied these algorithms to train different convolutional and residual neural networks, ranging from a shallow LeNet-like network to a self-built network with and without batch normalization layers and the modern ResNet-20, for image classification problems. We have compared the performance of both stochastic quasi-Newton trust-region methods with another stochastic quasi-Newton algorithm based on a progressive batching strategy and with the first-order Adam optimizer running with the optimal values of its hyperparameters, obtained by grid searching.

The rest of the paper is organized as follows: Section 2 provides a general overview of trust-region quasi-Newton methods for solving problem (1) and introduces the stochastic algorithms sL-BFGS-TR and sL-SR1-TR, together with a suitable minibatch sampling strategy. The results of an extensive empirical study on the performance of the considered algorithms in the training of deep neural networks are presented and discussed in Section 3. Finally, some concluding remarks are given in Section 4.

2. Materials and Methods

We provide in this section an overview of quasi-Newton trust-region methods in the deterministic setting and introduce suitable stochastic variants.

Trust-region (TR) methods [34] are powerful techniques for solving nonlinear unconstrained optimization problems that can incorporate second-order information, without re-

quiring it to be positive-definite. TR methods generate a sequence of iterates, $w_k + p_k$, such that the search direction p_k is obtained by solving the following TR subproblem,

$$p_k = \arg\min_{p \in \mathbb{R}^n} Q_k(p) \triangleq \frac{1}{2} p^T B_k p + g_k^T p \quad \text{s.t.} \quad \|p\|_2 \leq \delta_k, \tag{2}$$

for some TR radius $\delta_k > 0$, where

$$g_k \triangleq \nabla F(w_k) = \frac{1}{N} \sum_{i=1}^{N} \nabla L_i(w_k) \tag{3}$$

and B_k is a Hessian approximation. For quasi-Newton trust-region methods, the symmetric quasi-Newton (QN) matrices B_k in (2) are approximations to the Hessian matrix constructed using gradient information, and they satisfy the following secant equation:

$$B_{k+1} s_k = y_k, \tag{4}$$

where

$$s_k = p_k, \qquad y_k = g_t - g_k, \tag{5}$$

in which g_t is the gradient evaluated at $w_t = w_k + p_k$. The trial point is subject to the value of the ratio of actual to predicted reduction in the objective function of (1), that is:

$$\rho_k = \frac{f_k - f_t}{Q_k(0) - Q_k(p_k)}, \tag{6}$$

where f_t and f_k are the objective function values at w_t and w_k, respectively. Therefore, since the denominator in (6) is non-negative, if ρ_k is positive then $w_{k+1} \triangleq w_t$; otherwise, $w_{k+1} \triangleq w_k$. Based on the value of (6), the step may be accepted or rejected. Moreover, it is safe to expand $\delta_k \in (\delta_0, \delta_{max})$ with δ_0, $\delta_{max} > 0$ when there is very good agreement between the model and function. However, the current δ_k is not altered if there is good agreement, or it is shrunk when there is weak agreement. Algorithm 1 describes the TR radius adjustment.

Algorithm 1 Trust region radius adjustment

Inputs: Current iteration k, δ_k, ρ_k, $0 < \tau_2 < 0.5 < \tau_3 < 1$, $0 < \eta_2 \leq 0.5$, $0.5 < \eta_3 < 1 < \eta_4$
if $\rho_k > \tau_3$ **then**
  if $\|p_k\| \leq \eta_3 \delta_k$ **then**
    $\delta_{k+1} = \delta_k$
  else
    $\delta_{k+1} = \eta_4 \delta_k$
  end if
else if $\tau_2 \leq \rho_k \leq \tau_3$ **then**
  $\delta_{k+1} = \delta_k$
else
  $\delta_{k+1} = \eta_2 \delta_k$
end if

A primary advantage of using TR methods is their ability to work with both positive-definite and indefinite Hessian approximations. Moreover, the progress of the learning process will not stop or slow down even in the presence of occasional step rejection, i.e., when $w_{k+1} \triangleq w_k$.

Using the Euclidean norm (2-norm) to define the subproblem (2) leads to characterizing the global solution of (2) by the optimality conditions given in the following theorem from Gay [35] and Moré and Sorensen [36]:

Theorem 1. *Let δ_k be a given positive constant. A vector $p_k \triangleq p^*$ is a global solution of the trust region problem (2) if and only if $\|p^*\|_2 \leq \delta_k$ and there exists a unique $\sigma^* \geq 0$, such that $B_k + \sigma^* I$ is positive semi-definite with*

$$(B_k + \sigma^* I)p^* = -g_k, \quad \sigma^*(\delta_k - \|p^*\|_2) = 0. \tag{7}$$

Moreover, if $B_k + \sigma^* I$ is positive-definite, then the global minimizer is unique.

According to [37,38], the subproblem (2) or, equivalently, the optimality conditions (7) can be efficiently solved if the Hessian approximation B_k is chosen to be a QN matrix. In the following sections, we provide a comprehensive description of two methods in a TR framework with limited memory variants of two well-known QN Hessian approximations, i.e., L-BFGS and L-SR1.

2.1. The L-BFGS-TR Method

BFGS is the most popular QN update in the Broyden class; that is, it provides a Hessian approximation B_k, for which (4) holds. It has the following general form:

$$B_{k+1} = B_k - \frac{B_k s_k s_k^T B_k}{s_k^T B_k s_k} + \frac{y_k y_k^T}{y_k^T s_k}, \quad k = 0, 1, \ldots, \tag{8}$$

which is a positive-definite matrix, i.e., $B_{k+1} \succ 0$ if $B_0 \succ 0$ and the *curvature condition* holds, i.e., $s_k^T y_k > 0$. The difference between the symmetric approximations B_k and B_{k+1} is a rank-two matrix. In this work, we bypass updating B_k if the following curvature condition is not satisfied for $\tau = 10^{-2}$:

$$s_k^T y_k > \tau \|s_k\|^2. \tag{9}$$

For large-scale optimization problems, using the limited-memory BFGS (L-BFGS) would be more efficient. In practice, only a collection of the most recent pairs $\{s_j, y_j\}$ is stored in memory: for example, l pairs, where $l \ll n$ (usually $l < 100$). In fact, for $k \geq l$, the l recent computed pairs are stored in the following matrices S_k and Y_k:

$$S_k \triangleq \begin{bmatrix} s_{k-l} & s_{k-(l-1)} & \cdots & s_{k-1} \end{bmatrix}, \quad Y_k \triangleq \begin{bmatrix} y_{k-l} & y_{k-(l-1)} & \cdots & y_{k-1} \end{bmatrix}. \tag{10}$$

Using (10), the L-BFGS matrix B_k can be represented in the following compact form:

$$B_k = B_0 + \Psi_k M_k \Psi_k^T, \quad k = 1, 2, \ldots, \tag{11}$$

where $B_0 \succ 0$ and

$$\Psi_k = \begin{bmatrix} B_0 S_k & Y_k \end{bmatrix}, \qquad M_k = \begin{bmatrix} -S_k^T B_0 S_k & -L_k \\ -L_k^T & D_k \end{bmatrix}^{-1}. \tag{12}$$

We note that Ψ_k and M_k have at most $2l$ columns. In (12), matrices L_k, U_k, and D_k are, respectively, the strictly lower triangular part, the strictly upper triangular part, and the diagonal part of the following matrix splitting:

$$S_k^T Y_k = L_k + D_k + U_k. \tag{13}$$

Let $B_0 = \gamma_k I$. A heuristic and conventional method of choosing γ_k is

$$\gamma_k = \frac{y_{k-1}^T y_{k-1}}{y_{k-1}^T s_{k-1}} \triangleq \gamma_k^h. \tag{14}$$

The quotient of (14) is an approximation to an eigenvalue of $\nabla^2 F(w_k)$ and appears to be the most successful choice in practice [10]. Evidently, the selection of γ_k is important in generating Hessian approximations B_k. In DL optimization, the positive-definite L-

BFGS matrix B_k has the difficult task of approximating the possibly indefinite true Hessian. According to [29,30], an extra condition can be imposed on γ_k, to avoid false negative curvature information, i.e., to avoid $p_k^T B_k p_k < 0$ whenever $p_k^T \nabla^2(w_k) p_k > 0$. Let, for simplicity, the objective function of (1) be a quadratic function:

$$F(w) = \frac{1}{2} w^T H w + g^T w, \tag{15}$$

where $H = \nabla^2 F(w)$, which results in $\nabla F(w_{k+1}) - \nabla F(w_k) = H(w_{k+1} - w_k)$ and, thus, $y_k = H s_k$ for all k. Thus, we obtain $S_k^T Y_k = S_k^T H S_k$. For the quadratic model, and using (11), we obtain

$$S_k^T H S_k - \gamma_k S_k^T S_k = S_k^T \Psi_k M_k \Psi_k^T S_k. \tag{16}$$

According to (16), if H is not positive-definite, then its negative curvature information can be captured by $S_k^T \Psi_k M_k \Psi_k^T S_k$ as $\gamma_k > 0$. However, false curvature information can be produced when the γ_k value chosen is too large while H is positive-definite. To avoid this, γ_k is selected in $(0, \hat{\lambda})$, where $\hat{\lambda}$ is the smallest eigenvalue of the following generalized eigenvalue problem:

$$(L_k + D_k + L_k^T) u = \lambda S_k^T S_k u, \tag{17}$$

with L_k and D_k defined in (13). Therefore, if $\hat{\lambda} \leq 0$, then γ_k is the maximum value of 1 and γ_k^h defined in (14). Given γ_k, the compact form (11) is applied in (7), where both optimality conditions together are solved for $p_k \triangleq p_k^*$ through Algorithm A1 included in Appendix B. Then, according to the value of (6), the step $w_k + p_k$ may be accepted or rejected.

2.2. The L-SR1-TR Method

Another popular QN update in the Broyden class is the SR1 formula, which generates good approximations to the true Hessian matrix, often better than the BFGS approximations [10]. The SR1 updating formula verifying the secant condition (4) is given by

$$B_{k+1} = B_k + \frac{(y_k - B_k s_k)(y_k - B_k s_k)^T}{(y_k - B_k s_k)^T s_k}, \quad k = 0, 1, \ldots. \tag{18}$$

In this case, the difference between the symmetric approximations B_k and B_{k+1} is a rank-one matrix. To prevent the vanishing of the denominator in (18), a simple safeguard that performs well in practice is to simply skip the update if the denominator is small [10], i.e., $B_{k+1} = B_k$. Therefore, the update (18) is applied only if

$$|s^T (y_k - B_k s_k)| \geq \tau \|s_k\| \|y_k - B_k s_k\|, \tag{19}$$

where $\tau \in (0, 1)$ is small, say $\tau = 10^{-8}$. In (18), if B_k is positive-definite, B_{k+1} may not have the same property. Regardless of the sign of $y_k^T s_k$ for each k, the SR1 method generates a sequence of matrices that may be indefinite. We note that the value of the quadratic model in (2) evaluated at the descent direction p^* is always less if this direction is also a direction of negative curvature. Therefore, the ability to generate indefinite approximations can actually be regarded as one of the chief advantages of SR1 updates in non-convex settings, like in DL applications.

In the limited-memory version of the SR1 (L-SR1) update, as in L-BFGS, only the l most recent curvature pairs are stored in matrices S_k and Y_k defined in (10). Using S_k and Y_k, the L-SR1 matrix B_k can be represented in the following compact form:

$$B_k = B_0 + \Psi_k M_k \Psi_k^T, \quad k = 1, 2, , \ldots, \tag{20}$$

where $B_0 = \gamma_k I$ for some $\gamma_k \neq 0$ and

$$\Psi_k = Y_k - B_0 S_k, \qquad M_k = (D_k + L_k + L_k^T - S_k^T B_0 S_k)^{-1}. \tag{21}$$

In (21), L_k and D_k are, respectively, the strictly lower triangular part and the diagonal part of $S_k^T Y_k$. We note that Ψ_k and M_k in the L-SR1 update have, at most, l columns.

In [29], it was proven that the trust region subproblem solution becomes closely parallel to the eigenvector corresponding to the most negative eigenvalue of the L-SR1 approximation B_k. This shows the importance of B_k to be able to capture curvature information correctly. On the other hand, it was highlighted how the choice of $B_0 = \gamma_k I$ affects B_k; in fact, not choosing γ_k judiciously in relation to $\hat{\lambda}$, the smallest eigenvalue of (17), can have adverse effects. Selecting $\gamma_k > \hat{\lambda}$ can result in false curvature information. Moreover, if γ_k is too close to $\hat{\lambda}$ from below, then B_k becomes ill-conditioned. If γ_k is too close to $\hat{\lambda}$ from above, then the smallest eigenvalue of B_k becomes negatively large arbitrarily. According to [29], the following lemma suggests selecting γ_k near but strictly less than $\hat{\lambda}$, to avoid asymptotically poor conditioning while improving the negative curvature approximation properties of B_k.

Lemma 1. *For a given quadratic objective function* (15)*, let* $\hat{\lambda}$ *denote the smallest eigenvalue of the generalized eigenvalue problem* (17)*. Then, for all* $\gamma_k < \hat{\lambda}$*, the smallest eigenvalue of* B_k *is bounded above by the smallest eigenvalue of* H *in the span of* S_k*, i.e.,*

$$\lambda_{min}(B_k) \leq \min_{S_k v \neq 0} \frac{v^T S_k^T H S_k v}{v^T S_k^T S_k v}.$$

In this work, we set $\gamma_k = \max\{10^{-6}, 0.5\hat{\lambda}\}$ in the case where $\hat{\lambda} > 0$; otherwise, the γ_k is set to $\gamma_k = \min\{-10^{-6}, 1.5\hat{\lambda}\}$. Given γ_k, the compact form (20) is applied in (7), where the optimality conditions together are solved for p_k through Algorithm A2 included in Appendix B, using the spectral decomposition of B_k as well as the Sherman–Morrison–Woodbury formula [38]. Then, according to the value of (6), the step $w_k + p_k$ may be accepted or rejected.

2.3. Stochastic Variants of L-BFGS-TR and L-SR1-TR

The main motivation behind the use of stochastic optimization algorithms in deep learning may be traced back to the existence of a special type of redundancy due to similarity between the data points in (1). In addition, the computation of the true gradient is expensive and the computation of the true Hessian is not practical in large-scale DL problems. Indeed, depending on the available computing resources, it could take a prohibitive amount of time to process the whole set of data examples as a single batch at each iteration of a deterministic algorithm. That is why most of the optimizers in DL work in the stochastic regime. In this regime, the training set $\{(x_i, y_i)\}_{i=1}^N$ is divided randomly into multiple—e.g., $\bar{N}$—batches. Then, a stochastic algorithm uses a single batch J_k at iteration k to compute the required quantities, i.e., stochastic loss and stochastic gradient, as follows:

$$f_k^{J_k} \triangleq F^{J_k}(w_k) = \frac{1}{|J_k|} \sum_{i \in J_k^{idx}} L_i(w_k), \qquad g_k^{J_k} \triangleq \nabla F^{J_k}(w_k) = \frac{1}{|J_k|} \sum_{i \in J_k^{idx}} \nabla L_i(w_k), \tag{22}$$

where $bs \triangleq |J_k|$ and J_k^{idx} denote the size of J_k and the index set of the samples belonging to J_k, respectively. In other words, the stochastic QN extensions (sQN) are obtained by replacement of the full loss f_k and gradient g_k in (3) by $f_k^{J_k}$ and $g_k^{J_k}$, respectively, throughout the iterative process of the algorithms. The process of randomly taking J_k, computing the required quantities (22) for finding a search direction, and then updating w_k constitutes one single iteration of a stochastic algorithm. This process is repeated for a given number of batches until one epoch (i.e., one pass through the whole set of data samples) is completed. At that point, the dataset is shuffled and new batches are generated for the next epoch; see Algorithms 2 and 3 for a description of the stochastic algorithms sL-BFGS-TR and sL-SR1-TR, respectively.

Algorithm 2 sL-BFGS-TR

Inputs: $w_0 \in \mathbb{R}^n$, os, epoch_{max}, l, $\gamma_0 > 0$, c, $S_0 = Y_0 = [.]$, $0 < \tau, \tau_1 < 1$
for $k = 0, 1, \ldots$ **do**
  Take a random and uniform multi-batch J_k of size bs and compute $f_k^{J_k}$, $g_k^{J_k}$ by (22)
  if epoch $>$ epoch_{max} **then**
    Stop training
  end if
  Compute p_k using Algorithm A1
  Compute $w_t = w_k + p_k$ and $f_t^{J_k}$, $g_t^{J_k}$ by (22)
  Compute $(s_k, y_k) = (w_t - w_k, g_t^{J_k} - g_k^{J_k})$ and $\rho_k = \dfrac{f_t^{J_k} - f_k^{J_k}}{Q(p_k)}$
  if $\rho_k \geq \tau_1$ **then**
    $w_{k+1} = w_t$
  else
    $w_{k+1} = w_k$
  end if
  Update δ_k by Algorithm 1
  if $s_k^T y_k > \tau \|s_k\|^2$ **then**
    Update storage matrices S_{k+1} and Y_{k+1} by l recent $\{s_j, y_j\}_{j=k-l+1}^{k}$
    Compute the smallest eigenvalue $\hat{\lambda}$ of (17) for updating $B_0 = \gamma_k I$
    if $\hat{\lambda} > 0$ **then**
      $\gamma_{k+1} = \max\{1, c\hat{\lambda}\} \in (0, \hat{\lambda})$
    else
      Compute γ_k^h by (14) and set $\gamma_{k+1} = \max\{1, \gamma_k^h\}$
    end if
    Update Ψ_{k+1}, M_{k+1}^{-1} by (11)
  else
    Set $\gamma_{k+1} = \gamma_k$, $\Psi_{k+1} = \Psi_k$ and $M_{k+1}^{-1} = M_k^{-1}$
  end if
end for

Algorithm 3 sL-SR1-TR

Inputs: $w_0 \in \mathbb{R}^n$, os, epoch_{max}, l, $\gamma_0 > 0$, c, c_1, $S_0 = Y_0 = [.]$, $0 < \tau, \tau_1 < 1$
for $k = 0, 1, \ldots$ **do**
  Take a random and uniform multi-batch J_k of size bs and compute $f_k^{J_k}$, $g_k^{J_k}$ by (22)
  if epoch $>$ epoch_{max} **then**
    Stop training
  end if
  Compute p_k using Algorithm A2
  Compute $w_t = w_k + p_k$ and $f_t^{J_k}$, $g_t^{J_k}$ by (22)
  Compute $(s_k, y_k) = (w_t - w_k, g_t^{J_k} - g_k^{J_k})$ and $\rho_k = \dfrac{f_t^{J_k} - f_k^{J_k}}{Q(p_k)}$
  if $\rho_k \geq \tau_1$ **then**
    $w_{k+1} = w_t$
  else
    $w_{k+1} = w_k$
  end if
  Update δ_k by Algorithm 1
  if $|s^T(y_k - B_k s_k)| \geq \tau \|s_k\| \|y_k - B_k s_k\|$ **then**
    Update storage matrices S_{k+1} and Y_{k+1} by l recent $\{s_j, y_j\}_{j=k-l+1}^{k}$
    Compute the smallest eigenvalue $\hat{\lambda}$ of (17) for updating $B_0 = \gamma_k I$
    if $\hat{\lambda} > 0$ **then**
      $\gamma_{k+1} = \max\{c, c_1\hat{\lambda}\}$
    else
      $\gamma_{k+1} = \min\{-c, c_2\hat{\lambda}\}$
    end if
    Update Ψ_{k+1}, M_{k+1}^{-1} by (21)
  else
    Set $\gamma_{k+1} = \gamma_k$, $\Psi_{k+1} = \Psi_k$ and $M_{k+1}^{-1} = M_k^{-1}$
  end if
end for

Subsampling Strategy and Batch Formation

In a stochastic setting, as batches change from one iteration to the next, differences in stochastic gradients can cause the updating process to yield poor curvature estimates

(s_k, y_k). Therefore, updating B_k, whether as (11) or (20), may lead to unstable Hessian approximations. To address this issue, the following two approaches have been proposed in the literature. As a primary remedy [19], one can use the same batch, J_k, for computing curvature pairs, as follows:

$$(s_k, y_k) = (p_k, g_t^{J_k} - g_k^{J_k}), \tag{23}$$

where $g_t^{J_k} \triangleq \nabla F^{J_k}(w_t)$. We refer to this strategy as full-batch sampling. In this strategy, the stochastic gradient at w_t is computed twice: once in (23) and again to compute the subsequent step, i.e., $g_t^{J_{k+1}}$ if w_t is accepted; otherwise, $g_k^{J_{k+1}}$ is computed. As a cheaper alternative, an overlap sampling strategy was proposed in [27], in which only a common (overlapping) part between every two consecutive batches J_k and J_{k+1} is employed for computing y_k. Defining $O_k = J_k \cap J_{k+1} \neq \emptyset$ of size $os \triangleq |O_k|$, the curvature pairs are computed as

$$(s_k, y_k) = (p_k, g_t^{O_k} - g_k^{O_k}), \tag{24}$$

where $g_t^{O_k} \triangleq \nabla F^{O_k}(w_t)$. As O_k, and thus J_k, should be sizeable, this strategy is called multi-batch sampling. Both these approaches were originally considered for a stochastic algorithm using L-BFGS updates without and with line search methods, respectively. Progressive sampling approaches to use L-SR1 updates in a TR framework were instead considered, to train fully connected networks in [29,39]. More precisely, in [29], the curvature pairs and the model goodness ratio are computed as

$$(s_k, y_k) = (p_k, g_t^{J_k} - g_k^{J_k}), \qquad \rho_k = \frac{f_t^{J_k} - f_k^{J_k}}{Q_k(p_k)}, \tag{25}$$

such that $J_k = J_k \cap J_{k+1}$. Progressive sampling strategies may avoid acquiring noisy gradients by increasing the batch size at each iteration [31], which may lead to increased costs per iteration. A recent study of a non-monotone trust-region method with adaptive batch sizes can be found in [40]. In this work, we use fixed-size sampling for both methods.

We have examined the following two strategies to implement the considered sQN methods in a TR approach, in which the subsampled function and gradient evaluations are computed using a fixed-size batch per iteration. Let $O_k = J_k \cap J_{k+1} \neq \emptyset$; then, we can consider one of the following options:

- $(s_k, y_k) = (p_k, g_t^{J_k} - g_k^{J_k}), \qquad \rho_k = \frac{f_t^{J_k} - f_k^{J_k}}{Q_k(p_k)}.$
- $(s_k, y_k) = (p_k, g_t^{O_k} - g_k^{O_k}), \qquad \rho_k = \frac{f_t^{O_k} - f_k^{O_k}}{Q_k(p_k)}.$

Clearly, in both options, every two successive batches have an overlapping set (O_k), which helps to avoid extra computations in the subsequent iteration. We have performed experiments with both sampling strategies and have found that the L-SR1 algorithm fails to converge when using the second option. As this fact deserves further investigation, we have only used the first sampling option in this paper. Let $J_k = O_{k-1} \cup O_k$, where O_{k-1} and O_k are the overlapping samples of J_k with batches J_{k-1} and J_{k+1}, respectively. Moreover, the fixed-size batches are drawn without replacement, to ensure the whole dataset is visited in one epoch. We assume that $|O_{k-1}| = |O_k| = os$ and, thus, overlap ratio $or \triangleq \frac{os}{bs} = \frac{1}{2}$ (half overlapping). It is easy to see that $\bar{N} = \left\lfloor \frac{N}{os} \right\rfloor - 1$ indicates the number of batches in one epoch, where $\lfloor a \rfloor$ rounds a to the nearest integer less than or equal to a. To create $\bar{N}$ batches, we can consider the two following cases: $rs \triangleq \mathrm{mod}(N, os) = 0$ and $rs \triangleq \mathrm{mod}(N, os) \neq 0$, where the mod (modulo operation) of N and os returns the remainder after division of N and os. In the first case, all $\bar{N}$ batches are duplex, composed by two subsets, O_{k-1} and O_k, as $J_k = O_{k-1} \cup O_k$, while in the second case, the $\bar{N}$-th batch is a triple batch, defined as $J_k = O_{k-1} \cup R_k \cup O_k$, where R_k is a subset of size $rs \neq 0$ and other $\bar{N} - 1$ batches are duplex. In the former case, the required quantities for computing y_k and ρ_k at iteration k are determined as

$$f_k^{J_k} = or(f_k^{O_{k-1}} + f_k^{O_k})$$

and

$$g_k^{J_k} = or(g_k^{O_{k-1}} + g_k^{O_k}),$$

where $or = \frac{1}{2}$. In the latter case, the required quantities with respect to the last triple batch $J_k = O_{k-1} \cup R_k \cup O_k$ are computed as

$$f_k^{J_k} = or(f_k^{O_{k-1}} + f_k^{O_k}) + (1 - 2or) f_k^{R_k}$$

and

$$g_k^{J_k} = or(g_k^{O_{k-1}} + g_k^{O_k}) + (1 - 2or) g_k^{R_k},$$

where $or = \dfrac{os}{2os + rs}$. In this work, we have considered batches corresponding to the first case. Figure 1 schematically shows batches J_k and J_{k+1} at iterations k and $k+1$, respectively, and the overlapping parts in this case:

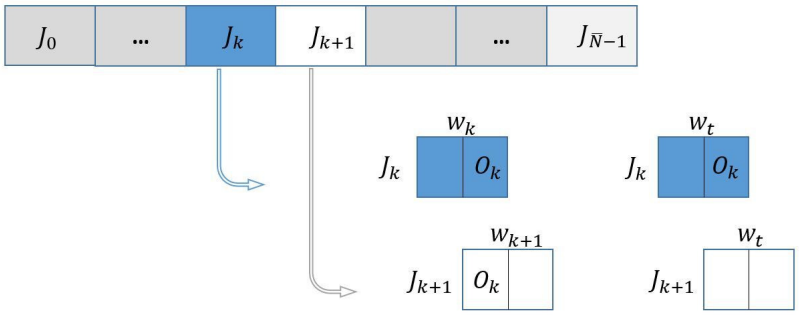

Figure 1. Fixed-size batches strategy scheme.

The stochastic loss value and gradient (22) are computed at the beginning (at w_k) and at the end of each iteration (at trial point w_t). In iteration $k+1$, these quantities have to be evaluated with respect to the sample subset represented by white rectangles only. In fact, the computations with respect to subset O_k at w_{k+1} depend on the acceptance status of w_t at iteration k. In the case of acceptance, the loss function and gradient vector have been already computed at w_t; in the case of rejection, these quantities are set equal to those evaluated at w_k, with respect to subset O_k.

3. Results

We present in this section the results of extensive experimentation to assess the effectiveness of the two described stochastic QN algorithms at solving the unconstrained optimization problems arising from the training of DNNs to accomplish image classification tasks. The deep learning toolbox of MATLAB provides a framework for designing and implementing a deep neural network, to perform image classification tasks using a prescribed training algorithm. We have exploited the deep learning custom training loops of MATLAB (https://www.mathworks.com/help/deeplearning/deep-learning-custom-training-loops.html, accessed on 15 October 2020), to implement Algorithms 2 and 3 with half-overlapping subsampling. The implementation details of the two stochastic QN algorithms considered in this work, using the DL toolbox of MATLAB (https://it.mathworks.com/help/deeplearning/, accessed on 15 October 2020), are provided in https://github.com/MATHinDL/sL_QN_TR/, where all the codes employed to obtain the numerical results included in this paper are also available.

To find an optimal classification model by using a C-class dataset, the generic problem (1) is solved by employing the softmax cross-entropy function, defined as

$$L_i(w) = -\sum_{k=1}^{C} (y_i)_k \log(h(x_i; w))_k,$$

for $i = 1, \ldots, N$. One of the most popular benchmarks for making informed decisions using data-driven approaches in DL is the MNIST dataset [41], as $\{(x_i, y_i)\}_{i=1}^{70,000}$, consisting of handwritten gray-scale images of digits x_i with 28×28 pixels taking values in $[0, 255]$ and its corresponding labels converted to one-hot vectors. Fashion-MNIST [42] is a variant of the original MNIST dataset, which shares the same image size and structure. Its images are assigned to fashion items (clothing) belonging also to 10 classes, but working with this dataset is more challenging than working with MNIST. The CIFAR-10 dataset [43] has 60,000 RGB images x_i of 32×32 pixels taking values in $[0, 255]$ in 10 classes. Every single image of the MNIST and Fashion-MNIST datasets is $x_i \in \mathbb{R}^{28\times28\times1}$, while the one of CIFAR10 is $x_i \in \mathbb{R}^{32\times32\times3}$. In all the datasets, 10,000 of the images are set aside as a testing set during training.

In this work, inspired by LeNet-5—mainly used for character recognition tasks [44]—we have used a LeNet-like network with a shallow structure. We have also employed a modern ResNet-20 residual network [45], exploiting special skip connections (shortcuts) to avoid possible gradient vanishing that might happen due to its deep architecture. Finally, we also consider a self-built convolutional neural network (CNN) named ConvNet3FC2 with a larger number of parameters than the two previous networks. To analyze the effect of batch normalization [46] on the performance of the stochastic QN algorithms, we have considered also variants of the ResNet-20 and ConvNet3FC2 networks, named ResNet-20 (No BN) and ConvNet3FC2 (No BN), in which the batch normalization layers have been removed. Table 1 describes the networks' architecture in detail. In this table, the syntax $(Conv(5 \times 5@32,\ 1, 2)/BN/ReLu/MaxPool(2 \times 2,\ 1, 0)))$ indicates a simple convolutional network (convnet) including a convolutional layer ($Conv$) using 32 filters of size 5×5, stride 1, padding 2, followed by a batch normalization layer (BN), a nonlinear activation function ($ReLu$) and, finally, a max-pooling layer with a channel of size 2×2, stride 1, and padding 0. The syntax $FC(C/Softmax)$ indicates a layer of C fully connected neurons followed by the *softmax* layer. Moreover, the syntax $addition(1)/Relu$ indicates the existence of an *identity shortcut* such that the output of a given block, say B_1 (or B_2 or B_3), is directly fed to the *addition* layer and then to the ReLu layer while $addition(2)/Relu$ in a block shows the existence of a *projection shortcut* by which the output from the two first convnets is added to the output of the third convnet and then the output is passed through the *ReLu* layer.

Table 2 shows the total number of trainable parameters, n, for different image classification problems. We have compared algorithms sL-BFGS-TR and sL-SR1-TR in training tasks for these problems. We have used the hyperparameters $c = 0.9$ and $\tau = 10^{-2}$ in sL-BFGS-TR, $c_1 = 0.5$, $c_2 = 1.5$, $c = 10^{-6}$, and $\tau = 10^{-8}$ in sL-SR1-TR, and $\tau_1 = 10^{-4}$, $\gamma_0 = 1$, $\tau_2 = 0.1$, $\tau_3 = 0.75$, $\eta_3 = 0.8$, $\eta_2 = 0.5$, and $\eta_4 = 2$ in both ones. We have also used the same initial parameter $w_0 \in \mathbb{R}^n$ by specifying the same seed to the MATLAB random number generator for both methods. All deep neural networks have been trained for at most 10 epochs, and training was terminated if 100% accuracy was reached.

The accuracy is the ratio of the number of correct predictions to the number of total predictions. In our study, we report the accuracy in percentage and overall loss values for both the train and the test datasets. Following prior published works in the optimization community (see, e.g., [28]) we use the whole testing set as the validation set: that is, at the end of each iteration of the training phase (after the network parameters have been updated) the prediction capability of the recently updated network is evaluated, using all the samples of the test dataset. The computed value is the measured testing accuracy corresponding to iteration k. Consequently, we report accuracy and loss across epochs for both the training samples and the unseen samples of the validation set (=the test set) during the training phase.

To facilitate visualization, we plot the measurement under evaluation versus epochs, using a determined frequency of display, which is reported at the top of the figures. Display frequency values larger than one indicate the number of iterations that are not reported, while all the iterations are considered if the display frequency is one. All the figures report the results of a single run; see also the additional experiments in the Supplementary Material.

Table 1. Networks.

LeNet-like	
Structure	$(Conv(5 \times 5@20,\ 1,0)/ReLu/MaxPool(2 \times 2,\ 2,0))$
	$(Conv(5 \times 5@50,\ 1,0)/ReLu/MaxPool(2 \times 2,\ 2,0))$
	$FC(500/ReLu)$
	$FC(C/Softmax)$
ResNet-20	
Structure	$(Conv(3 \times 3@16,\ 1,1)/BN/ReLu)$
	$B_1 \begin{cases} (Conv(3 \times 3@16,\ 1,1)/BN/ReLu) \\ (Conv(3 \times 3@16,\ 1,1)/BN) + addition(1)/Relu \end{cases}$ $B_2 \begin{cases} (Conv(3 \times 3@16,\ 1,1)/BN/ReLu) \\ (Conv(3 \times 3@16,\ 1,1)/BN) + addition(1)/Relu \end{cases}$ $B_3 \begin{cases} (Conv(3 \times 3@16,\ 1,1)/BN/ReLu) \\ (Conv(3 \times 3@16,\ 1,1)/BN) + addition(1)/Relu \end{cases}$
	$B_1 \begin{cases} (Conv(3 \times 3@32,\ 2,1)/BN/ReLu) \\ (Conv(3 \times 3@32,\ 1,1)/BN) \\ (Conv(1 \times 1@32,\ 2,0)/BN) + addition(2)/Relu \end{cases}$ $B_2 \begin{cases} (Conv(3 \times 3@32,\ 1,1)/BN/ReLu) \\ (Conv(3 \times 3@32,\ 1,1)/BN) + addition(1)/Relu \end{cases}$ $B_3 \begin{cases} (Conv(3 \times 3@32,\ 1,1)/BN/ReLu) \\ (Conv(3 \times 3@32,\ 1,1)/BN) + addition(1)/Relu \end{cases}$
	$B_1 \begin{cases} (Conv(3 \times 3@64,\ 2,1)/BN/ReLu) \\ (Conv(3 \times 3@64,\ 1,1)/BN) \\ (Conv(1 \times 1@64,\ 2,0)/BN) + addition(2)/Relu \end{cases}$ $B_2 \begin{cases} (Conv(3 \times 3@64,\ 1,1)/BN/ReLu) \\ (Conv(3 \times 3@64,\ 1,1)/BN) + addition(1)/Relu \end{cases}$ $B_3 \begin{cases} (Conv(3 \times 3@64,\ 1,1)/BN/ReLu) \\ (Conv(3 \times 3@64,\ 1,1)/BN) + addition(1)/g.AvgPool/ReLu) \end{cases}$
	$FC(C/Softmax)$
ConvNet3FC2	
Structure	$(Conv(5 \times 5@32,\ 1,2)/BN/ReLu/MaxPool(2 \times 2,\ 1,0))$
	$(Conv(5 \times 5@32,\ 1,2)/BN/ReLu/MaxPool(2 \times 2,\ 1,0))$
	$(Conv(5 \times 5@64,\ 1,2)/BN/ReLu/MaxPool(2 \times 2,\ 1,0))$
	$FC(64,/BN/ReLu)$
	$FC(C/Softmax)$

Table 2. The total number of the networks' trainable parameters (n).

	LeNet-5	**ResNet-20**	**ResNet-20 (No BN)**	**ConvNet3FC2**	**ConvNet3FC2 (No BN)**
MNIST	431,030	272,970	271,402	2,638,826	2,638,442
F.MNIST	431,030	272,970	271,402	2,638,826	2,638,442
CIFAR10	657,080	273,258	271,690	3,524,778	3,525,162

We have performed extensive testing to analyze different aspects that may influence the performance of the two considered stochastic QN algorithms: mainly, the limited memory parameter and the batch size. We have also compared the performance of both algorithms from the point of view of CPU time. Finally, we have provided a comparison with first- and second-order methods. All experiments were performed on a Ubuntu Linux server virtual machine with 32 CPUs and 128 GB RAM.

3.1. Influence of the Limited Memory Parameter

The results reported in Figure 2 illustrate the effect of the limited memory parameter value ($l = 5, 10$ and 20) on the accuracy achieved by the two stochastic QN algorithms in training ConvNet3FC2 on CIFAR10 within a fixed number of epochs. As is clearly shown in this figure, in particular for ConvNet3FC2 (No BN), the effect of the limited memory parameter is more pronounced when large batches are used ($bs = 5000$). For large batch sizes, the larger the value of l, the higher the accuracy. No remarkable differences in the behavior of both algorithms with a small batch size ($bs = 500$) are observed. It seems that incorporating more recently computed curvature vectors (i.e., larger l) does not increase the efficiency of the algorithms in training DNNs with BN layers, while it does when BN layers are removed. Finally, we remark that we have found that using larger values of l ($l \geq 30$) is not helpful, having led to higher over-fitting in some of our experiments.

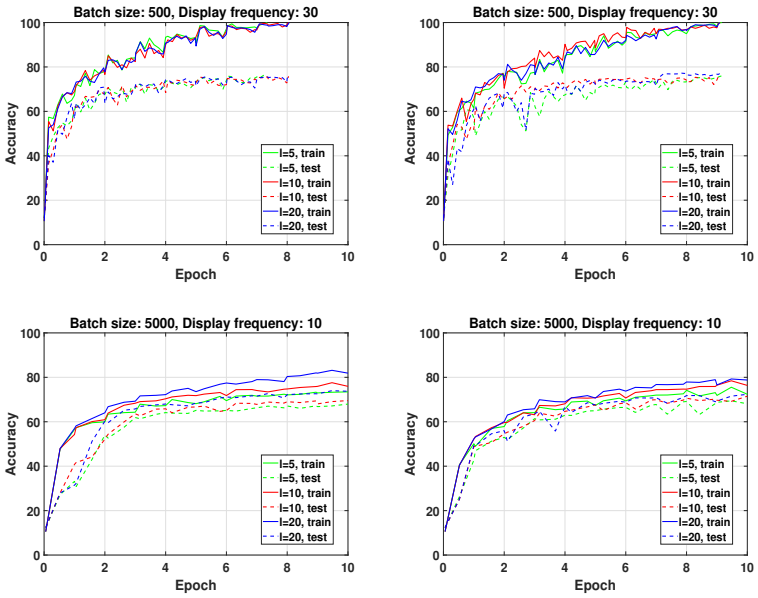

(a) CIFAR10 with ConvNet3FC2

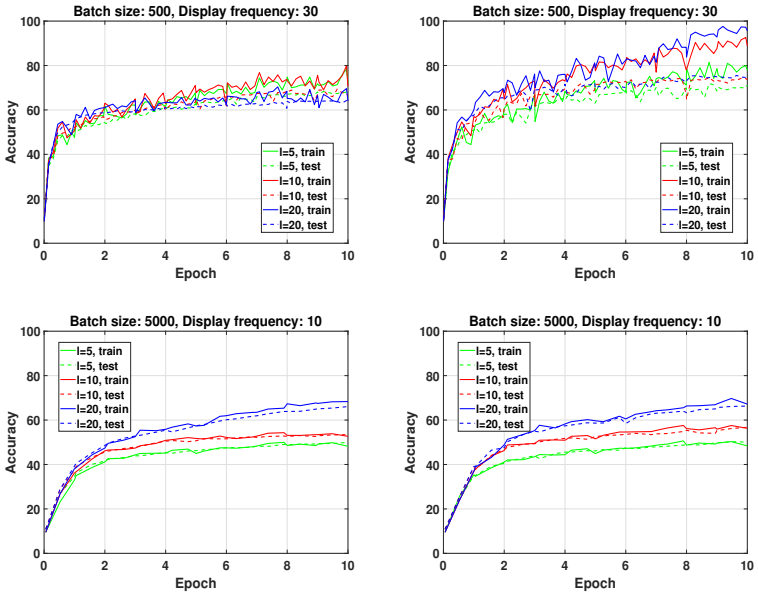

(b) CIFAR10 with ConvNet3FC2(no BN)

Figure 2. The performance of sL-BFGS-TR (**left**) and sL-SR1-TR (**right**) with different limited memory values (l).

3.2. Influence of the Batch Size

In this subsection, we analyze the effect of the batch size on the performance of the two considered sQN methods, while keeping fixed the limited memory parameter $l = 20$. We have considered different values of the batch size (bs) in $\{100, 500, 1000, 5000\}$ or, equivalently, overlap size (os) in $\{50, 250, 500, 2500\}$ for all the problems and all the considered DNNs. Based on Figure 3, the general conclusion is that when training the networks for a fixed number of epochs, the achieved accuracy decreases when the batch size increases. This is due to the reduction in the number of parameter updates. We have summarized in Table 3 the relative superiority of one of the two stochastic QN algorithms over the other for all problems. With "both", we indicate that both algorithms display similar behavior. From the results reported in Table 3, we conclude that sL-SR1-TR performs better than sL-BFGS-TR for training networks without BN layers, while both QN updates exhibit comparable performances when used for training networks with BN layers. More detailed comments for each DNN are given below.

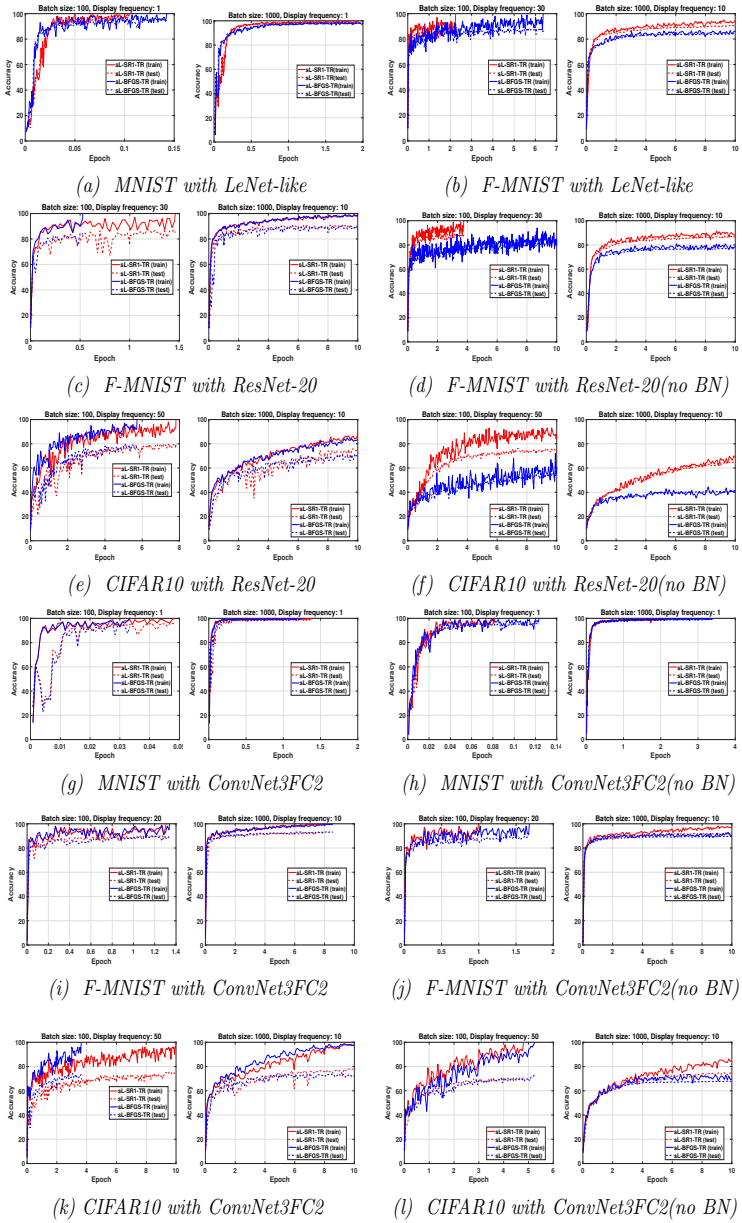

(a) MNIST with LeNet-like *(b) F-MNIST with LeNet-like*

(c) F-MNIST with ResNet-20 *(d) F-MNIST with ResNet-20(no BN)*

(e) CIFAR10 with ResNet-20 *(f) CIFAR10 with ResNet-20(no BN)*

(g) MNIST with ConvNet3FC2 *(h) MNIST with ConvNet3FC2(no BN)*

(i) F-MNIST with ConvNet3FC2 *(j) F-MNIST with ConvNet3FC2(no BN)*

(k) CIFAR10 with ConvNet3FC2 *(l) CIFAR10 with ConvNet3FC2(no BN)*

Figure 3. Evolution of the training and testing accuracy for batch sizes 100 and 1000 ($l = 20$).

Table 3. Summary of the best sQN approach for each combination problem/network architecture.

	LeNet-5	ResNet-20	ResNet-20 (No BN)	ConvNet3FC2	ConvNet3FC2 (No BN)
MNIST	sL-SR1-TR	both	sL-SR1-TR	both	both
F.MNIST	sL-SR1-TR	both	sL-SR1-TR	both	sL-SR1-TR
CIFAR10	sL-SR1-TR	sL-BFGS-TR	sL-SR1-TR	sL-BFGS-TR	sL-SR1-TR

3.2.1. LeNet-like

The results on top of Figure 3 show that both the algorithms perform well, in training LeNet-like within 10 epochs to classify MNIST and Fashion-MNIST datasets, respectively. Specifically, sL-SR1-TR provides better classification accuracy than sL-BFGS-TR.

3.2.2. ResNet-20

Figure 3 shows that the classification accuracy on Fashion-MNIST increases when using ResNet-20 instead of LeNet-like, as expected. Regarding the performance of the two algorithms of interest, both algorithms exhibit comparable performances when BN is used. Nevertheless, we point out the fact that sL-BFGS-TR using $bs = 100$ achieves higher accuracy than sL-SR1-TR, in less time. This comes with some awkward oscillations in the testing curves. We attribute these oscillations to a sort of inconsistency between the updated parameters and the normalized features of the testing set samples. This is due to the fact that the inference step by testing samples is done using the updated parameters and the features that are normalized by the most recently computed mean and variance moving average values obtained by the batch normalization layers in the training phase [46]. The numerical results on ResNet-20 without the BN layers confirm this assumption can be true. These results also show that sL-SR1-TR performs better than sL-BFGS-TR in this case. Note that the experiments on LeNet-like and ResNet-20 with and without BN layers show that sL-SR1-TR performs better than sL-BFGS-TR when batch normalization is not used, but, as can be clearly seen from the results, the elimination of the BN layers causes a detriment to all the methods' performances.

3.2.3. ConvNet3FC2

Figure 3 shows that sL-BFGS-TR still produces better testing/training accuracy than sL-SR1-TR on CIFAR10, while both algorithms behave similarly on the MNIST and Fashion-MNIST datasets. In addition, sL-BFGS-TR with $bs = 100$ within 10 epochs achieves the highest accuracy faster than sL-SR1-TR (see Figure 3k).

3.3. Comparison with Adam Optimizer

Adaptive moment estimation (Adam) [7] is a popular efficient first-order optimizer used in DL. Due to the high sensitivity of Adam to the value of its hyperparameters, it is usually used after the determination of near-optimal values through grid searching strategies, which is a very time-consuming task. It is worth noting that sL-QN-TR approaches do not require step-length tuning, and this particular experiment offers a comparison to optimized Adam. To compare sL-BFGS-TR and sL-SR1-TR to Adam, we have performed a grid search on learning rates and batch sizes, to select the best value of Adam's hyperparameters. We have considered learning rates values in $\{10^{-5}, 10^{-4}, 10^{-3}, 10^{-2}, 10^{-1}, 1\}$ and batch size in $\{100, 500, 1000, 5000\}$, and we have selected the pair of values that allows Adam to achieve the highest testing accuracy. The gradient and squared gradient decay factors are set as $\beta_1 = 0.9$ and $\beta_2 = 0.999$, respectively. The small constant for preventing divide-by-zero errors is set to 10^{-8}.

Figure 4 illustrates the results obtained with the two considered sQN algorithms and the tuned Adam. We have analyzed which algorithm achieves the highest training accuracy within, at most, 10 epochs for different batch sizes. In networks using BN layers, all methods achieve comparable training and testing accuracy within 10 epochs with $bs = 1000$. However, this cannot be generally observed when $bs = 100$. The figure

shows that tuned Adam provides higher testing accuracy than sL-SR1-TR. Nevertheless, sL-BFGS-TR is still faster at achieving the highest training accuracy, as we also previously observed. It also provides testing accuracy comparable to tuned Adam. On the other hand, for networks without BN layers, sL-SR1-TR is the clear winner.

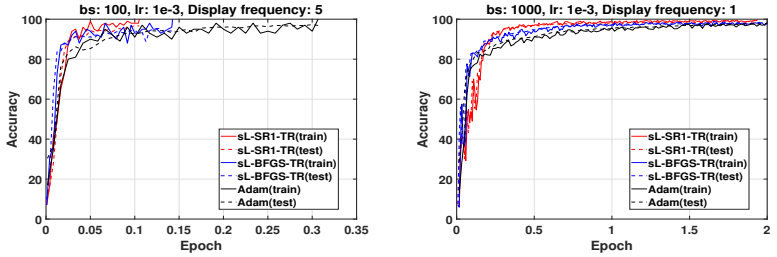

(a) MNIST with LeNet-like

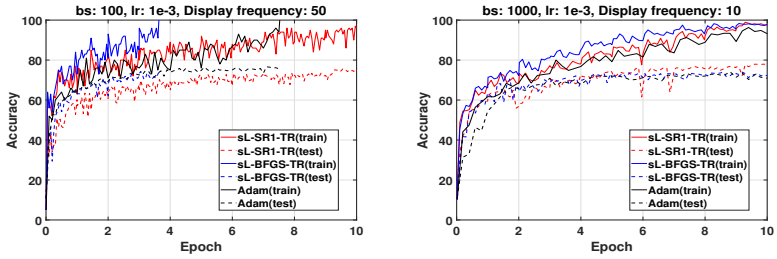

(b) CIFAR10 with ConvNet3FC2

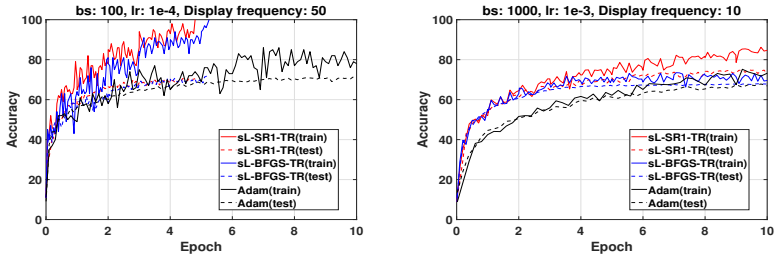

(c) CIFAR10 with ConvNet3FC2(no BN)

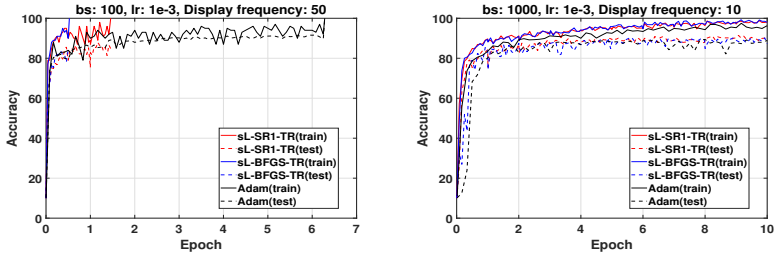

(d) Fashion-MNIST with ResNet-20

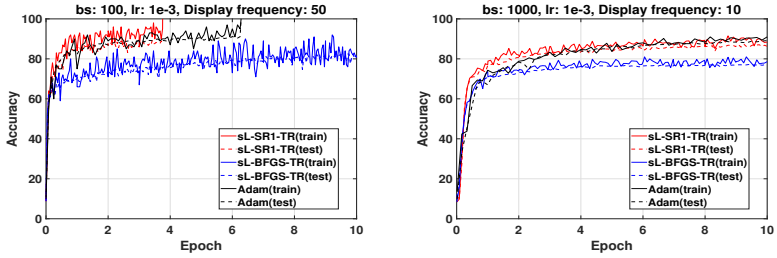

(e) Fashion-MNIST with ResNet-20(no BN)

Figure 4. Comparison of sL-BFGS-TR, sL-SR1-TR (both with $l = 20$) and tuned Adam (with optimal learning rate lr) for different batch sizes (bs). Learning rates equal to 10^{-4} and 10^{-3} are indicated as `lr: 1e-3` and `lr: 1e-4`, respectively.

A final remark is that Adam's performance seems to be more negatively affected by large minibatch size than QN methods. For this reason, QN methods can increase their advantage over Adam when using large batch sizes to enhance the parallel efficiency of distributed implementations.

3.4. Comparison with STORM

We have performed a comparison between our sQN training algorithms and the algorithm STORM (Algorithm 5 in [47]). STORM relies on an adaptive batching strategy aimed at avoiding inaccurate stochastic function evaluations in the TR framework. Note that the real reduction of the objective function is not guaranteed in a stochastic-trust-region approach. In [32,47], the authors claim that if the stochastic functions are sufficiently accurate, this will increase the number of true successful iterations. Therefore, they considered a progressive sampling strategy with sample size

$$b_k = \min(N, \max(b_0 \cdot k + b_1, \lceil \frac{1}{{\delta_k}^2} \rceil)),$$

where δ_k is the trust region radius at iteration k, N is the total number of samples, and b_0, b_1 are $b_0 = 100$, $b_1 = 32 \times 32 \times 3$ for CIFAR10, and $b_1 = 28 \times 28 \times 1$ for Fashion-MNIST.

We have applied STORM with both L-SR1 and L-BFGS updates. We have compared the performances of the sL-SR1-TR and sL-BFGS-TR algorithms employing different overlapping batch sizes running for 10 epochs with the performance provided by STORM with progressive batch size b_k running for 50 epochs. We allowed STORM to execute for more epochs, i.e., 50 epochs, since, due to its progressive sampling behavior it passed 10 epochs very rapidly. The largest batch size reached by STORM within this number of epochs is near $b_k = 25{,}000$ (i.e., 50 percent of the total number of training samples).

The results of this experiment are summarized in Figure 5. In both Fashion-MNIST and CIFAR10 problems, the algorithms with $bs = 500$ and $bs = 1000$ produce comparable or higher final accuracy than STORM at the end of their respective training phases. Even if we set a fixed budget of time corresponding to the one needed by STORM to perform 50 epochs, sL-QN-TR algorithms with $bs = 500$ and $bs = 1000$ provide comparable or higher accuracy. The results corresponding to the smallest and largest batch sizes need a separate discussion. When $bs = 100$, the stochastic QN algorithms are not better than STORM with any fixed budget of time; however, they provide higher final training accuracy and testing accuracy, except for the Fashion-MNIST problem on ResNet-20 trained by sL-BFGS-TR.

By contrast, when $bs = 5000$, sL-BFGS-TR algorithms produce higher or comparable training accuracy but not a testing accuracy comparable to the one provided by STORM. This seems quite logical, as using such a large batch size causes the algorithms to perform a small number of iterations and then to update the parameter vector only a few times; allowing longer training time or more epochs can compensate for this lower accuracy. Finally, this experiment shows also that the sL-BFGS-TR algorithm with $bs = 5000$ yields higher accuracy within less time than that obtained when $bs = 100$ is used.

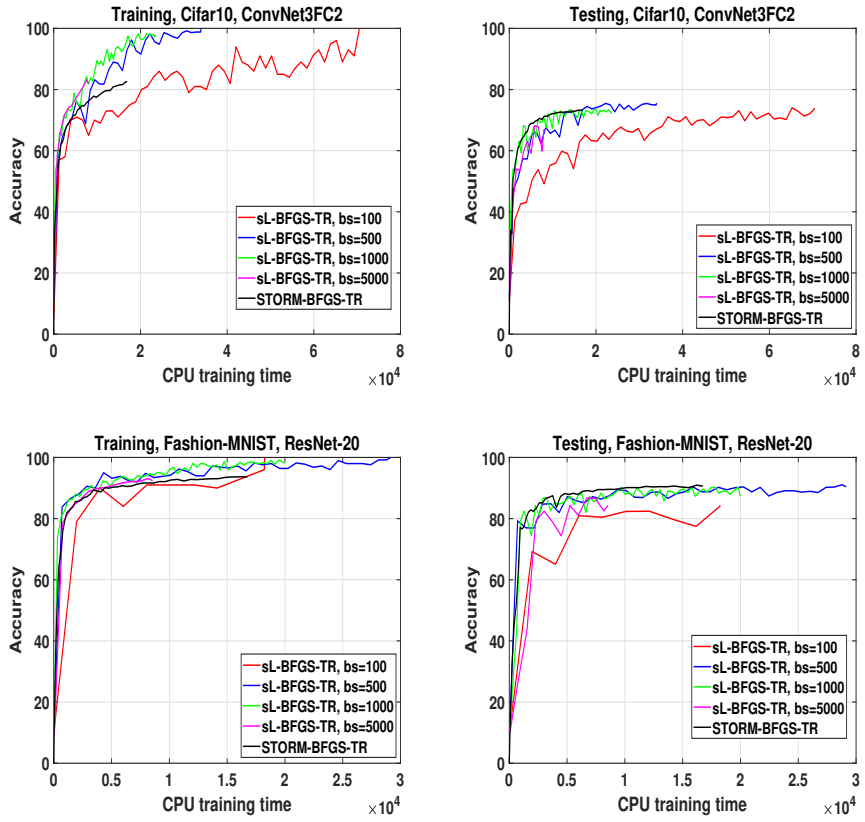

(a) sL-BFGS-TR

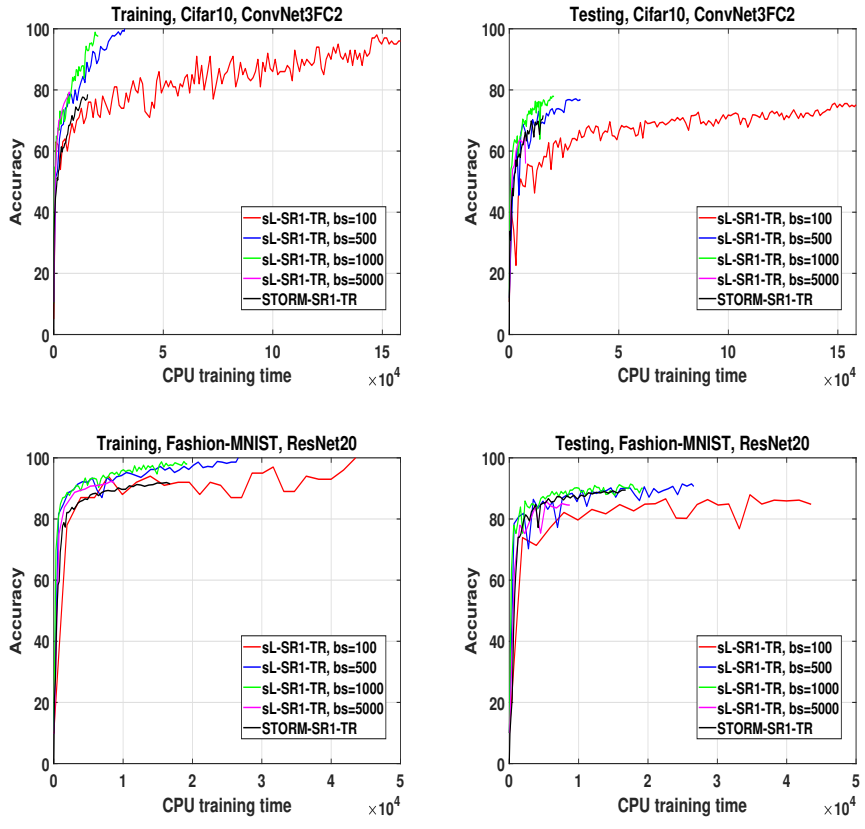

(b) sL-SR1-TR

Figure 5. The performance of sL-BFGS-TR and sL-SR1-TR with different fixed batch sizes (*bs*), in comparison to STORM. Left and right columns display the Training and Testing accuracies, respectively.

4. Conclusions

We have studied stochastic QN methods for training deep neural networks. We have considered both L-SR1 and L-BFGS updates in a stochastic setting in a trust region framework. Extensive experimental work—including the effect of batch normalization (BN), the limited memory parameter, the sampling strategy, and batch size—has been reported and discussed. Our experiments show that BN is a key factor in the performance of stochastic QN algorithms and that sL-BFGS-TR behaves comparably to or slightly better than sL-SR1-TR when BN layers are used, while sL-SR1-TR performs better in networks without BN layers. This behavior is in accordance with the property of L-SR1 updates allowing for indefinite Hessian approximations in non-convex optimization. However, the exact reason for the different behavior of the two stochastic QN algorithms with networks not employing BN layers is not completely clear and would deserve further investigation.

The reported experimental results have illustrated that employing larger batch sizes within a fixed number of epochs produces lower training accuracy, which can be recovered by longer training. Regarding training time, our results have also shown a slight superiority in the accuracy reached by both algorithms when larger batch sizes are used within a fixed budget of time. This suggests the use of large batch sizes also in view of the parallelization of the algorithms.

The proposed sQN algorithms, with the overlapping fixed-size sampling strategy, revealed to be more efficient than the adaptive progressive batching algorithm STORM, which naturally incorporates a variance reduction technique.

Finally, our results show that sQN methods are efficient in practice and, in some instances, outperform tuned Adam. We believe that this contribution fills a gap concerning the real performance of the SR1 and BFGS updates in realistic large-size DNNs, and it is expected to help steer the researchers in this field towards the option of the proper quasi-Newton method.

Supplementary Materials: The following supporting information can be downloaded at: https://www.mdpi.com/article/10.3390/a16100490/s1. The following supporting information includes additional numerical results for different image classification problems, enhancing the comprehensive nature of our study. Figure S1: `MNIST`, `LeNet-like`: Accuracy and loss evolution vs. epoch. Figure S2: `F-MNIST`, `LeNet-like`: Accuracy and loss evolution vs. epoch. Figure S3: `F-MNIST`, `ResNet-20`: Accuracy and loss evolution vs. epoch. Figure S4: `CIFAR10`, `ResNet-20`: Accuracy and loss evolution vs. epoch. Figure S5: `F-MNIST`, `ResNet-20 (No BN)`: Accuracy and loss evolution vs. epoch. Figure S6: `CIFAR10`, `ResNet-20 (No BN)`: Accuracy and loss evolution vs. epoch. Figure S7: `MNIST`, `ConvNet3FC2`: Accuracy and loss evolution vs. epoch. Figure S8: `F-MNIST`, `ConvNet3FC2`: Accuracy and loss evolution vs. epoch. Figure S9: `CIFAR10`, `ConvNet3FC2`: Accuracy and loss evolution vs. epoch. Figure S10: `MNIST`, `ConvNet3FC2 (No BN)`: Accuracy and loss evolution vs. epoch. Figure S11: `F-MNIST`, `ConvNet3FC2 (No BN)`: Accuracy and loss evolution vs. epoch. Figure S12: `CIFAR10`, `ConvNet3FC2 (No BN)`: Accuracy and loss evolution vs. epoch. Figure S13: `MNIST` and `F-MNIST`: Accuracy evolution vs. CPU time. Figure S14: `CIFAR10`: Accuracy evolution vs. CPU time. Figure S15: `MNIST`, `LeNet-like`: Comparison with tuned Adam. Figure S16: `F-MNIST`, `ResNet-20`: Comparison with tuned Adam. Figure S17: `F-MNIST`, `ResNet-20 (No BN)`: `ResNet-20`: Comparison with tuned Adam. Figure S18: `CIFAR10`, `ConvNet3FC2`: Comparison with tuned Adam. Figure S19: `CIFAR10`, `ConvNet3FC2 (No BN)`: Comparison with tuned Adam.

Author Contributions: Conceptualization, Á.M. and M.Y; methodology, Á.M. and M.Y; software implementation, M.Y.; validation, Á.M.; writing—original draft preparation, Á.M. and M.Y; writing of manuscript Á.M. and M.Y; supervision, review, and editing Á.M. All authors have read and agreed to the published version of the manuscript.

Funding: This research received no funding.

Data Availability Statement: The datasets utilized in this research are publicly accessible and commonly employed benchmarks in the field of machine learning and deep learning, see [41–43].

Acknowledgments: Á.M. and M.Y. gratefully acknowledge the support of the INdAM-GNCS Project CUP_E53C22001930001. The work of Á.M. was carried out within the PNRR research activities of the consortium iNEST (Interconnected North-Est Innovation Ecosystem) funded by the European Union Next-GenerationEU (Piano Nazionale di Ripresa e Resilienza (PNRR)—Missione 4 Componente 2, Investimento 1.5—D.D. 1058 23 June 2022, ECS_00000043). This manuscript reflects only the authors' views and opinions; neither the European Union nor the European Commission can be considered responsible for them.

Conflicts of Interest: The authors declare no conflict of interest.

Appendix A. Solvers for the TR Subproblem

Appendix A.1. Computing with an L-BFGS Matrix

This section describes how to solve the TR subproblem (2), using L-BFGS through Algorithm A1; see [30,38,48] for more details. Let B_k be an L-BFGS compact matrix (11). Using Theorem 1, the global solution of the TR subproblem (2) can be obtained by exploiting the following two strategies:

Spectral Decomposition of B_k

By the thin QR factorization of the matrix Ψ_k, $\Psi_k = Q_k R_k$, or the Cholesky factorization of the matrix $\Psi_k^T \Psi_k$, $\Psi_k^T \Psi_k = R^T R$, and then spectral decomposition of the small matrix $R_k M_k R_k^T$ as $R_k M_k R_k^T = U_k \hat{\Lambda} U_k^T$, we have

$$B_k = B_0 + Q_k R_k M_k R_k^T Q_k^T = \gamma_k I + Q_k U_k \hat{\Lambda} U_k^T Q_k^T,$$

where U_k and $\hat{\Lambda}$, respectively, are orthogonal and diagonal matrices. Now, let $P_{\|} \triangleq Q_k U_k$ (or let $P_{\|} \triangleq (\Psi_k R_k^{-1} U_k)^T$) and $P_{\perp} \triangleq (Q_k U_k)^{\perp}$, where $\perp$ is an orthogonal complement (perpendicular). By Theorem 2.1.1 in [49], we obtain $P^T P = P P^T = I$, where

$$P \triangleq \begin{bmatrix} P_{\|} & P_{\perp} \end{bmatrix} \in \mathbb{R}^{n \times n}. \tag{A1}$$

Therefore, the spectral decomposition of B_k is obtained as

$$B_k = P \Lambda P^T, \qquad \Lambda \triangleq \begin{bmatrix} \Lambda_1 & 0 \\ 0 & \Lambda_2 \end{bmatrix} = \begin{bmatrix} \hat{\Lambda} + \gamma_k I & 0 \\ 0 & \gamma_k I \end{bmatrix}, \tag{A2}$$

where $\Lambda = \operatorname{diag}(\hat{\lambda}_1, \ldots, \hat{\lambda}_n) = \operatorname{diag}(\hat{\lambda}_1 + \gamma_k, \ldots, \hat{\lambda}_k + \gamma_k, \gamma_k, \ldots, \gamma_k) \in \mathbb{R}^{n \times n}$ with $\Lambda_1 \in \mathbb{R}^{2l \times 2l}$ and $\Lambda_2 \in \mathbb{R}^{(n-2l) \times (n-2l)}$ when $k > 2l$. We note that $\Lambda_1 \in \mathbb{R}^{k \times k}$ and $\Lambda_2 \in \mathbb{R}^{(n-k) \times (n-k)}$ when $k \leq 2l$. We also assume the eigenvalues in Λ_1 are ordered in increasing values. Notice that Λ_1 includes, at most, $2l$ elements with limited memory parameter l.

Inversion by Sherman–Morrison–Woodbury Formula

By dropping subscript k in (11) and using the Sherman–Morrison–Woodbury formula to compute the inverse of the coefficient matrix in (7), we obtain

$$p(\sigma) = -(B + \sigma I)^{-1} g = -\frac{1}{\tau} \left(I - \Psi \left(\tau M^{-1} + \Psi^T \Psi \right)^{-1} \Psi^T \right) g, \tag{A3}$$

where $\tau = \gamma + \sigma$. By using (A2), the first optimality condition in (7) can be written as

$$(\Lambda + \sigma I) v = -P^T g, \tag{A4}$$

where

$$v = P^T p, \qquad P^T g \triangleq \begin{bmatrix} g_{\|} \\ g_{\perp} \end{bmatrix} = \begin{bmatrix} P_{\|}^T g \\ P_{\perp}^T g \end{bmatrix}, \tag{A5}$$

and, therefore,

$$\|p(\sigma)\| = \|v(\sigma)\| = \sqrt{\left\{\sum_{i=1}^{k} \frac{(g_{\|})_i^2}{(\lambda_i + \sigma)^2}\right\} + \frac{\|g_{\perp}\|^2}{(\gamma + \sigma)^2}}, \tag{A6}$$

where $\|g_{\perp}\|^2 = \|g\|^2 - \|g_{\|}\|^2$. This makes the computation of $\|p\|$ feasible without computing p explicitly. Let $p_u \triangleq p(0)$ as an unconstrained minimizer for (2) be the solution of the first optimality condition in (7), for which $\sigma = 0$ makes the second optimality condition hold. Now, we consider the following cases. If $\|p_u\| \leq \delta$, the optimal solution of (2) using (A3) is computed as

$$(\sigma^*, p^*) = (0, p_u) = (0, p(0)). \tag{A7}$$

If $\|p_u\| > \delta$, then p^* must lie on the boundary of the TR, to hold the second optimality condition. To impose this, σ^* must be the root of the following equation, which is determined by the Newton method proposed in [38]:

$$\phi(\sigma) \triangleq \frac{1}{\|p(\sigma)\|} - \frac{1}{\delta} = 0. \tag{A8}$$

Therefore, using (A3), the global solution is computed as

$$(\sigma^*, p^*) = (\sigma^*, p(\sigma^*)). \tag{A9}$$

Appendix A.2. Computing with an L-SR1 Matrix

For solving (2), where B_k is a compact L-SR1 matrix (20), the efficient Algorithm A2, called the Orthonormal Basis L-SR1 (OBS), was proposed in [38]. Let (A2) be the eigenvalue decomposition of (20), where $\Lambda = \text{diag}(\hat{\lambda}_1, \ldots, \hat{\lambda}_n) = \text{diag}(\hat{\lambda}_1 + \gamma_k, \ldots, \hat{\lambda}_k + \gamma_k, \gamma_k, \ldots, \gamma_k) \in \mathbb{R}^{n \times n}$ with $\Lambda_1 \in \mathbb{R}^{l \times l}$ and $\Lambda_2 \in \mathbb{R}^{(n-l)\times(n-l)}$ when $k > l$. We note that $\Lambda_1 \in \mathbb{R}^{k \times k}$ and $\Lambda_2 \in \mathbb{R}^{(n-k)\times(n-k)}$ when $k \leq l$. We also assume the eigenvalues in Λ_1 are ordered in increasing values. Note that Λ_1 includes, at most, l elements with limited memory parameter l. The OBS method exploits the Sherman–Morrison–Woodbury formula in different cases for L-SR1 B_k; by dropping subscript k in (20), these cases are:

B is positive-definite

In this case, the global solution of (2) is (A7) or (A9).

B is positive semi-definite (singular)

As $\gamma \neq 0$ and B is positive semi-definite with all non-negative eigenvalues, then $\lambda_{min} = \min\{\lambda_1, \gamma\} = \lambda_1 = 0$. Let r be the multiplicity of λ_{min}; therefore,

$$0 = \lambda_1 = \lambda_2 = \cdots = \lambda_r < \lambda_{r+1} \leq \lambda_{r+2} \leq \cdots \leq \lambda_k.$$

For $\sigma > -\lambda_{min} = 0$, the matrix $(\Lambda + \sigma I)$ in (A4) is invertible and, thus, $\|p(\sigma)\|$ in (A6) is well defined. For $\sigma = -\lambda_{min} = 0$, we consider the two following sub-cases to have a well-defined expression in (A6); we will discuss in the limit setting at $-\lambda_{min}^{+}$. If $\lim_{\sigma \to 0^+} \phi(\sigma) < 0$, then $\lim_{\sigma \to 0^+} \|p(\sigma)\| > \delta$. Here, the OBS algorithm uses Newton's method to find $\sigma^* \in (0, \infty)$, so that the global solution p^* lies on the boundary of the trust region, i.e., $\phi(\sigma^*) = 0$. This solution $p^* = p(\sigma^*)$ is computed using (A3), by which, the global pair solution (σ^*, p^*) satisfies the first and second optimal conditions in (7). If $\lim_{\sigma \to 0^+} \phi(\sigma) \geq 0$, then $\lim_{\sigma \to 0^+} \|p(\sigma)\| \leq \delta$. It can be proved that $\phi(\sigma)$ is strictly increasing for $\sigma > 0$ (see Lemma 7.3.1 in [34]). This makes $\phi(\sigma) \geq 0$ for $\sigma > 0$, as it is non-negative at 0^+ and, thus, $\phi(\sigma)$ can only have a root $\sigma^* = 0$ in $\sigma \geq 0$. Here, we should note that even if $\phi(\sigma) > 0$, the solution $\sigma^* = 0$ makes the second optimality condition in (7) hold. As matrix $B + \sigma I$

at $\sigma^* = 0$ is not invertible, the global solution p^* for the first optimality condition in (7) is computed by

$$\begin{aligned} p^* = p(\sigma^*) &= -(B + \sigma^* I)^\dagger g = -P(\Lambda + \sigma^* I)^\dagger P^T g \\ &= -P_\parallel (\Lambda_1 + \sigma^* I)^\dagger P_\parallel^T g - \frac{1}{\gamma + \sigma^*} P_\perp P_\perp^T g \\ &= -\Psi R^{-1} U (\Lambda_1 + \sigma^* I)^\dagger g_\parallel - \frac{1}{\gamma + \sigma^*} P_\perp P_\perp^T g, \end{aligned} \tag{A10}$$

where $(g_\parallel)_i = (P_\parallel^T g)_i = 0$ for $i = 1, \ldots, r$ if $\sigma^* = -\lambda_{min} = -\lambda_1 = 0$, and

$$P_\perp P_\perp^T g = (I - P_\parallel P_\parallel^T) g = (I - \Psi R^{-1} R^{-T} \Psi^T) g.$$

Therefore, both optimality conditions in (7) hold for the pair solution (σ^*, p^*).

B is indefinite

Let r be the algebraic multiplicity of the leftmost eigenvalue λ_{min}. As B is indefinite and $\gamma \neq 0$, we obtain $\lambda_{min} = \min\{\lambda_1, \gamma\} < 0$.

Evidently, for $\sigma > -\lambda_{min}$, the matrix $(\Lambda + \sigma I)$ in (A4) is invertible and, thus, $\|p(\sigma)\|$ in (A6) is well defined. For $\sigma = -\lambda_{min}$, we discuss the two following cases. If $\lim_{\sigma \to -\lambda_{min}^+} \phi(\sigma) < 0$, then $\lim_{\sigma \to -\lambda_{min}^+} \|p(\sigma)\| > \delta$. The OBS algorithm uses Newton's method, to find $\sigma^* \in (-\lambda_{min}, \infty)$ as the root of $\phi(\sigma) = 0$, so that the global solution p^* lies on the boundary of the trust region. By using (A3) to compute $p^* = p(\sigma^*)$, the pair (σ^*, p^*) satisfies both the conditions in (7). If $\lim_{\sigma \to -\lambda_{min}^+} \phi(\sigma) \geq 0$, then $\lim_{\sigma \to -\lambda_{min}^+} \|p(\sigma)\| \geq \delta$. For $\sigma > -\lambda_{min}$, we obtain $\phi(\sigma) \geq 0$, but the solution $\sigma^* = -\lambda_{min}$ as the only root of $\phi(\sigma) = 0$ is a positive number, which cannot satisfy the second optimal condition when $\phi(\sigma)$ is strictly positive. Hence, we should consider the cases of equality and inequality separately:

Equality. Let $\lim_{\sigma \to -\lambda_{min}^+} \phi(\sigma) = 0$. As matrix $B + \sigma I$ at $\sigma^* = -\lambda_{min}$ is not invertible, the global solution p^* for the first optimality condition in (7) is computed using (A10) by

$$p^* = \begin{cases} -\Psi R^{-1} U (\Lambda_1 + \sigma^* I)^\dagger g_\parallel - \dfrac{1}{\gamma + \sigma^*} P_\perp P_\perp^T g, & \sigma^* \neq -\gamma, \\ -\Psi R^{-1} U (\Lambda_1 + \sigma^* I)^\dagger g_\parallel, & \sigma^* = -\gamma, \end{cases} \tag{A11}$$

where $g_\perp = P_\perp^T g = 0$ and, thus, $\|g_\perp\| = 0$ if $\sigma^* = -\lambda_{min} = -\gamma$. For $i = 1, \ldots, r$, we obtain $(g_\parallel)_i = (P_\parallel^T g)_i = 0$ if $\sigma^* = -\lambda_{min} = -\lambda_1$.

We note that both optimality conditions in (7) hold for the computed (σ^*, p^*).

Inequality. Let $\lim_{\sigma \to -\lambda_{min}^+} \phi(\sigma) > 0$; then, $\lim_{\sigma \to -\lambda_{min}^+} \|p(\sigma)\| < \delta$. As mentioned above, $\sigma = -\lambda_{min} > 0$ cannot satisfy the second optimality condition. In this case, a so-called *hard case*, we attempt to find a solution that lies on the boundary. For $\sigma^* = -\lambda_{min}$, this optimal solution is provided by

$$p^* = \hat{p}^* + z^*, \tag{A12}$$

where $\hat{p}^* = -(B + \sigma^* I)^\dagger g$ is computed by (A11) and $z^* = \alpha u_{min}$. Vector u_{min} is a unit eigenvector in the subspace associated with λ_{min}, and α is obtained so that $\|p^*\| = \delta$, i.e.,

$$\alpha = \sqrt{\delta^2 - \|\hat{p}^*\|^2}. \tag{A13}$$

The computation of u_{min} depends on $\lambda_{min} = \min\{\lambda_1, \gamma\}$. If $\lambda_{min} = \lambda_1$, then the first column of P is a leftmost eigenvector of B and, thus, u_{min} is set to the first column of $P_{\|}$. On the other hand, if $\lambda_{min} = \gamma$, then any vector in the column space of $P_{\perp}$ will be an eigenvector of B corresponding to λ_{min}. However, we avoid forming matrix $P_{\perp}$ to compute $P_{\perp}P_{\perp}^T g$ in (A11) if $\lambda_{min} = \lambda_1$. By definition (A1), we have that

$$\text{Range}(P_{\perp}) = \text{Range}(P_{\|})^{\perp}, \qquad \text{Range}(P_{\|}) = \text{Ker}(I - P_{\|}P_{\|}^T).$$

To find a vector in the column space of $P_{\perp}$, we use $I - P_{\|}P_{\|}^T$ as a projection matrix mapping onto the column space of $P_{\perp}$. For simplicity, we can map one canonical basis vector at a time onto the column space of $P_{\perp}$ until a nonzero vector is obtained. This practical process, repeated, at most, $k+1$ times, will result in a vector that lies in $\text{Range}(P_{\perp})$, i.e.,

$$u_{min} \triangleq (I - P_{\|}P_{\|}^T)e_j, \tag{A14}$$

for $j = 1, 2, \ldots k+1$ with $\|u_{min}\| \neq 0$; because $e_j \in \text{Range}(P_{\|})$ and

$$\text{rank}(P_{\|}) = \dim \text{Range}(P_{\|}) = \dim \text{Kerl}(I - P_{\|}P_{\|}^T) = k.$$

In this process, we start with $e_1 \in \text{Range}(P_{\|})$, such that

$$(I - P_{\|}P_{\|}^T)e_1 \in \text{Range}(P_{\perp}).$$

If $\|(I - P_{\|}P_{\|}^T)e_1\| \neq 0$, the vector u_{min} is found; otherwise, we map the next canonical basis vector, e_2. If $(I - P_{\|}P_{\|}^T)e_j = 0$ and, thus, $\|(I - P_{\|}P_{\|}^T)e_j\| = 0$, for $j = 1, \ldots, k$, then u_{min} is obtained in the attempt $j = k+1$.

Appendix B. Trust-Region Subproblem Solution Algorithms

Algorithm A1 TR subproblem solution with an L-BFGS compact matrix.

Inputs:
Current iteration k, $\delta \triangleq \delta_k$, $g \triangleq g_k$ and $B \triangleq B_k$: $\Psi \triangleq \Psi_k$, $M^{-1} \triangleq M_k^{-1}$, $\gamma \triangleq \gamma_k$
Compute the thin QR factors Q and R of Ψ or the Cholesky factor R of $\Psi^T\Psi$
Compute the spectral decomposition of matrix RMR^T, i.e., $RMR^T = U\hat{\Lambda}U^T$
Set $\hat{\Lambda} = \text{diag}(\hat{\lambda}_1, \ldots, \hat{\lambda}_k)$ such that $\hat{\lambda}_1 \leq \ldots \leq \hat{\lambda}_k$ and $\lambda_{min} = \min\{\lambda_1, \gamma\}$
Compute the spectral of B_k as $\Lambda_1 = \hat{\Lambda} + \gamma I$
Compute $P_{\|} = QU$ or $P_{\|} = (\Psi R^{-1}U)^T$ and $g_{\|} = P_{\|}^T g$
if $\phi(0) \geq 0$ **then**
    Set: $\sigma^* = 0$
    Compute p^* with (A3) as solution of $(B_k + \sigma^* I)p = -g$
else
    Compute a root $\sigma^* \in (0, \infty)$ of (A8) by Newton method [38]
    Compute p^* with (A3) as solution of $(B_k + \sigma^* I)p = -g$
end if

Algorithm A2 TR subproblem solution with an L-SR1 compact matrix.

Inputs:
Current iteration k, $\delta \triangleq \delta_k$, $g \triangleq g_k$ and $B \triangleq B_k$: $\Psi \triangleq \Psi_k$, $M^{-1} \triangleq M_k^{-1}$, $\gamma \triangleq \gamma_k$
Compute the thin QR factors Q and R of Ψ or the Cholesky factor R of $\Psi^T\Psi$
Compute the spectral decomposition of matrix RMR^T, i.e., $RMR^T = U\hat{\Lambda}U^T$
Set $\hat{\Lambda} = \text{diag}(\hat{\lambda}_1, \ldots, \hat{\lambda}_k)$ such that $\hat{\lambda}_1 \leq \ldots \leq \hat{\lambda}_k$ and $\lambda_{min} = \min\{\lambda_1, \gamma\}$
Compute the spectral of B_k as $\Lambda_1 = \hat{\Lambda} + \gamma I$
Compute $P_{\|} = QU$ or $P_{\|} = (\Psi R^{-1}U)^T$ and $g_{\|} = P_{\|}^T g$
if Case I: $\lambda_{min} > 0$ and $\phi(0) \geq 0$ **then**
    Set: $\sigma^* = 0$
    Compute p^* with (A3) as solution of $(B_k + \sigma^* I)p = -g$
else if Case II: $\lambda_{min} \leq 0$ and $\phi(-\lambda_{min}) \geq 0$ **then**
    Set: $\sigma^* = -\lambda_{min}$
    Compute p^* with (A10) as solution of $(B_k + \sigma^* I)p = -g$
    if Case III: $\lambda_{min} < 0$ **then**
        Compute α and u_{min} with (A12) for $z^* = \alpha u_{min}$
        Update: $p^* = p^* + z^*$
    end if
else
    Compute a root $\sigma^* \in (\max\{-\lambda_{min}, 0\}, \infty)$ of (A8) by Newton method [38]
    Compute p^* with (A3) as solution of $(B_k + \sigma^* I)p = -g$
end if

References

1. Robbins, H.; Monro, S. A stochastic approximation method. *Ann. Math. Stat.* **1951**, *22*, 400–407. [CrossRef]
2. Bottou, L.; LeCun, Y. Large-scale online learning. *Adv. Neural Inf. Process. Syst.* **2004**, *16*, 217–224.
3. Defazio, A.; Bach, F.; Lacoste-Julien, S. SAGA: A fast incremental gradient method with support for non-strongly convex composite objectives. In Proceedings of the Advances in Neural Information Processing Systems, Montreal, QC, Canada, 8–13 December 2014; pp. 1646–1654.
4. Johnson, R.; Zhang, T. Accelerating stochastic gradient descent using predictive variance reduction. *Adv. Neural Inf. Process. Syst.* **2013**, *26*, 315–323.
5. Schmidt, M.; Le Roux, N.; Bach, F. Minimizing finite sums with the stochastic average gradient. *Math. Program.* **2017**, *162*, 83–112. [CrossRef]
6. Duchi, J.; Hazan, E.; Singer, Y. Adaptive subgradient methods for online learning and stochastic optimization. *J. Mach. Learn. Res.* **2011**, *12*, 2121–2159.
7. Kingma, D.P.; Ba, J. Adam: A method for stochastic optimization. In Proceedings of the 3rd International Conference on Learning Representations, ICLR 2015—Conference Track Proceedings, San Diego, CA, USA, 7–9 May 2015.
8. Ziyin, L.; Li, B.; Ueda, M. SGD May Never Escape Saddle Points. *arXiv* **2021**, arXiv:2107.11774.
9. Kylasa, S.; Roosta, F.; Mahoney, M.W.; Grama, A. GPU accelerated sub-sampled Newton's method for convex classification problems. In Proceedings of the 2019 SIAM International Conference on Data Mining, SIAM, Calgary, AB, Canada, 2–4 May 2019; pp. 702–710.
10. Nocedal, J.; Wright, S. *Numerical Optimization*; Springer Series in Operations Research and Financial Engineering; Springer Science & Business Media: Berlin/Heidelberg, Germany, 2006.
11. Bottou, L.; Curtis, F.E.; Nocedal, J. Optimization methods for large-scale machine learning. *SIAM Rev.* **2018**, *60*, 223–311. [CrossRef]
12. Martens, J. Deep learning via Hessian-Free optimization. In Proceedings of the ICML, Haifa, Israel, 21–24 June 2010; Volume 27, pp. 735–742.
13. Martens, J.; Sutskever, I. Training deep and recurrent networks with Hessian-Free optimization. In *Neural Networks: Tricks of the Trade*; Springer: Berlin/Heidelberg, Germany, 2012; pp. 479–535.
14. Bollapragada, R.; Byrd, R.H.; Nocedal, J. Exact and inexact subsampled Newton methods for optimization. *IMA J. Numer. Anal.* **2019**, *39*, 545–578. [CrossRef]
15. Xu, P.; Roosta, F.; Mahoney, M.W. Second-order optimization for non-convex machine learning: An empirical study. In Proceedings of the 2020 SIAM International Conference on Data Mining, SIAM, Cincinnati, OH, USA, 7–9 May 2020; pp. 199–207.
16. Steihaug, T. The conjugate gradient method and trust-regions in large-scale optimization. *SIAM J. Numer. Anal.* **1983**, *20*, 626–637. [CrossRef]

17. Jahani, M.; Nazari, M.; Rusakov, S.; Berahas, A.S.; Takáč, M. Scaling up Quasi-Newton algorithms: Communication efficient distributed SR1. In Proceedings of the Machine Learning, Optimization, and Data Science: 6th International Conference, LOD 2020, Siena, Italy, 19–23 July 2020; Revised Selected Papers, Part I 6; Springer: Berlin/Heidelberg, Germany, 2020; pp. 41–54.
18. Berahas, A.S.; Jahani, M.; Richtárik, P.; Takáč, M. Quasi-Newton methods for machine learning: Forget the past, just sample. *Optim. Methods Softw.* **2022**, *37*, 1668–1704. [CrossRef]
19. Schraudolph, N.N.; Yu, J.; Günter, S. A stochastic Quasi-Newton method for online convex optimization. In Proceedings of the Artificial Intelligence and Statistics, PMLR, San Juan, PR, USA, 21–24 March 2007; pp. 436–443.
20. Byrd, R.H.; Hansen, S.L.; Nocedal, J.; Singer, Y. A stochastic Quasi-Newton method for large-scale optimization. *SIAM J. Optim.* **2016**, *26*, 1008–1031. [CrossRef]
21. Moritz, P.; Nishihara, R.; Jordan, M. A linearly-convergent stochastic L-BFGS algorithm. In Proceedings of the Artificial Intelligence and Statistics, PMLR, Cadiz, Spain, 9–11 May 2016; pp. 249–258.
22. Gower, R.; Goldfarb, D.; Richtárik, P. Stochastic block BFGS: Squeezing more curvature out of data. In Proceedings of the International Conference on Machine Learning, PMLR, Cadiz, Spain, 9–11 May 2016; pp. 1869–1878.
23. Mokhtari, A.; Ribeiro, A. RES: Regularized stochastic BFGS algorithm. *IEEE Trans. Signal Process.* **2014**, *62*, 6089–6104. [CrossRef]
24. Mokhtari, A.; Ribeiro, A. Global convergence of online limited memory BFGS. *J. Mach. Learn. Res.* **2015**, *16*, 3151–3181.
25. Lucchi, A.; McWilliams, B.; Hofmann, T. A variance reduced stochastic Newton method. *arXiv* **2015**, arXiv:1503.08316.
26. Wang, X.; Ma, S.; Goldfarb, D.; Liu, W. Stochastic Quasi-Newton methods for nonconvex stochastic optimization. *SIAM J. Optim.* **2017**, *27*, 927–956. [CrossRef]
27. Berahas, A.S.; Nocedal, J.; Takáč, M. A multi-batch L-BFGS method for machine learning. *Adv. Neural Inf. Process. Syst.* **2016**, *29*, 1055–1063. [CrossRef]
28. Berahas, A.S.; Takáč, M. A robust multi-batch L-BFGS method for machine learning. *Optim. Methods Softw.* **2020**, *35*, 191–219. [CrossRef]
29. Erway, J.B.; Griffin, J.; Marcia, R.F.; Omheni, R. Trust-region algorithms for training responses: Machine learning methods using indefinite Hessian approximations. *Optim. Methods Softw.* **2020**, *35*, 460–487. [CrossRef]
30. Rafati, J.; Marcia, R.F. Improving L-BFGS initialization for trust-region methods in deep learning. In Proceedings of the 2018 17th IEEE International Conference on Machine Learning and Applications (ICMLA), Orlando, FL, USA, 17–20 December 2018; IEEE: New York, NY, USA, 2018; pp. 501–508.
31. Bollapragada, R.; Nocedal, J.; Mudigere, D.; Shi, H.J.; Tang, P.T.P. A progressive batching L-BFGS method for machine learning. In Proceedings of the International Conference on Machine Learning, PMLR, Stockholm, Sweden, 10–15 July 2018; pp. 620–629.
32. Blanchet, J.; Cartis, C.; Menickelly, M.; Scheinberg, K. Convergence rate analysis of a stochastic trust-region method via supermartingales. *INFORMS J. Optim.* **2019**, *1*, 92–119. [CrossRef]
33. Goldfarb, D.; Ren, Y.; Bahamou, A. Practical Quasi-Newton methods for training deep neural networks. *Adv. Neural Inf. Process. Syst.* **2020**, *33*, 2386–2396.
34. Conn, A.R.; Gould, N.I.; Toint, P.L. *Trust-Region Methods*; SIAM: Philadelphia, PA, USA, 2000. Available online: https://epubs.siam.org/doi/book/10.1137/1.9780898719857 (accessed on 1 November 2020).
35. Gay, D.M. Computing optimal locally constrained steps. *SIAM J. Sci. Stat. Comput.* **1981**, *2*, 186–197. [CrossRef]
36. Moré, J.J.; Sorensen, D.C. Computing a trust-region step. *SIAM J. Sci. Stat. Comput.* **1983**, *4*, 553–572. [CrossRef]
37. Burdakov, O.; Gong, L.; Zikrin, S.; Yuan, Y.x. On efficiently combining limited-memory and trust-region techniques. *Math. Program. Comput.* **2017**, *9*, 101–134. [CrossRef]
38. Brust, J.; Erway, J.B.; Marcia, R.F. On solving L-SR1 trust-region subproblems. *Comput. Optim. Appl.* **2017**, *66*, 245–266. [CrossRef]
39. Wang, X.; Yuan, Y.X. Stochastic trust-region methods with trust-region radius depending on probabilistic models. *arXiv* **2019**, arXiv:1904.03342.
40. Krejic, N.; Jerinkic, N.K.; Martínez, A.; Yousefi, M. A non-monotone extra-gradient trust-region method with noisy oracles. *arXiv* **2023**, arXiv:2307.10038.
41. LeCun, Y. The MNIST Database of Handwritten Digits. 1998. Available online: https://www.kaggle.com/datasets/hojjatk/mnist-dataset (accessed on 1 November 2020).
42. Xiao, H.; Rasul, K.; Vollgraf, R. Fashion-MNIST: A novel image dataset for benchmarking machine learning algorithms. *arXiv* **2017**, arXiv:1708.07747.
43. Krizhevsky, A.; Hinton, G. Learning Multiple Layers of Features from Tiny Images. 2009. Available online: https://www.cs.toronto.edu/~kriz/cifar.html (accessed on 1 November 2020).
44. LeCun, Y.; Bottou, L.; Bengio, Y.; Haffner, P. Gradient-based learning applied to document recognition. *Proc. IEEE* **1998**, *86*, 2278–2324. [CrossRef]
45. He, K.; Zhang, X.; Ren, S.; Sun, J. Deep residual learning for image recognition. In Proceedings of the IEEE Conference on Computer Vision and Pattern Recognition, Las Vegas, NV, USA, 27–30 June 2016; pp. 770–778.
46. Ioffe, S.; Szegedy, C. Batch normalization: Accelerating deep network training by reducing internal covariate shift. In Proceedings of the International Conference on Machine Learning, PMLR, Lille, France, 7–9 July 2015; pp. 448–456.

47. Chen, R.; Menickelly, M.; Scheinberg, K. Stochastic optimization using a trust-region method and random models. *Math. Program.* **2018**, *169*, 447–487. [CrossRef]
48. Adhikari, L.; DeGuchy, O.; Erway, J.B.; Lockhart, S.; Marcia, R.F. Limited-memory trust-region methods for sparse relaxation. In Proceedings of the Wavelets and Sparsity XVII. International Society for Optical Engineering, San Diego, CA, USA, 6–9 August 2017; Volume 10394.
49. Golub, G.H.; Van Loan, C.F. *Matrix Computations*, 4th ed.; Johns Hopkins University Press: Baltimore, MD, USA, 2013.

Disclaimer/Publisher's Note: The statements, opinions and data contained in all publications are solely those of the individual author(s) and contributor(s) and not of MDPI and/or the editor(s). MDPI and/or the editor(s) disclaim responsibility for any injury to people or property resulting from any ideas, methods, instructions or products referred to in the content.